

CERN-EP-2023-106
30 May 2023

Accessing the strong interaction between Λ baryons and charged kaons with the femtoscopy technique at the LHC

ALICE Collaboration*

Abstract

The interaction between Λ baryons and kaons/antikaons is a crucial ingredient for the strangeness $S = 0$ and $S = -2$ sector of the meson–baryon interaction at low energies. In particular, the $\Lambda\bar{K}$ might help in understanding the origin of states such as the $\Xi(1620)$, whose nature and properties are still under debate. Experimental data on Λ – K and Λ – \bar{K} systems are scarce, leading to large uncertainties and tension between the available theoretical predictions constrained by such data. In this Letter we present the measurements of Λ – $K^+ \oplus \bar{\Lambda}$ – K^- and Λ – $K^- \oplus \bar{\Lambda}$ – K^+ correlations obtained in the high-multiplicity triggered data sample in pp collisions at $\sqrt{s} = 13$ TeV recorded by ALICE at the LHC. The correlation function for both pairs is modeled using the Lednický–Lyuboshits analytical formula and the corresponding scattering parameters are extracted. The Λ – $K^- \oplus \bar{\Lambda}$ – K^+ correlations show the presence of several structures at relative momenta k^* above 200 MeV/ c , compatible with the Ω baryon, the $\Xi(1690)$, and $\Xi(1820)$ resonances decaying into Λ – K^- pairs. The low k^* region in the Λ – $K^- \oplus \bar{\Lambda}$ – K^+ also exhibits the presence of the $\Xi(1620)$ state, expected to strongly couple to the measured pair. The presented data allow to access the ΛK^+ and ΛK^- strong interaction with an unprecedented precision and deliver the first experimental observation of the $\Xi(1620)$ decaying into ΛK^- .

© 2023 CERN for the benefit of the ALICE Collaboration.

Reproduction of this article or parts of it is allowed as specified in the CC-BY-4.0 license.

*See Appendix A for the list of collaboration members

1 Introduction

Measurements of correlations of particle pairs in the relative momentum space performed in small colliding systems at the Large Hadron Collider (LHC), such as proton–proton (pp) and p–Pb collisions, have proven to be a sensitive experimental tool to investigate hadron–hadron interactions. In recent years, this so-called femtoscopy technique [1] was employed by the ALICE Collaboration to deliver a large amount of high-precision data on interactions involving strange baryons and antibaryons [2–9]. This made it possible to validate for the first time state-of-the-art lattice QCD predictions at the physical point and to provide crucial experimental tests for low-energy effective field theories. Lately, the same technique was applied to meson–baryon pairs giving the possibility to access the interaction of protons with ϕ , charm D mesons, and kaons [10–13]. In the strangeness $S = -1$ meson–baryon sector, the measurement of the K^-p correlation function in different colliding systems [12–14] provided a detailed picture of the K^-p strong interaction above threshold and novel constraints on the coupling strength to the \bar{K}^0n and $\pi\Sigma$ channels. These femtoscopic correlations delivered the most precise data on the K^-p interaction and a crucial input to pin down the $\bar{K}N-\pi\Sigma$ dynamics, responsible for the formation of the $\Lambda(1405)$ resonance [15–17], which currently is the only accepted molecular state in the hadronic spectrum.

States with a similar nature, namely arising dynamically in multi-channel interactions, are predicted to exist also in the $S = -2$ meson–baryon sector in which antikaons (\bar{K}) interact with the strange Λ baryon. Theoretical calculations based on chiral unitary frameworks [18–22], Bethe-Salpeter approaches [23], and meson-exchange models [24] indicate that several Ξ resonances, such as the $\Xi(1620)$ and the $\Xi(1690)$, might indeed originate from the coupling between the $\Lambda-\bar{K}$ system and other $S = -2$ channels, like $\pi\Xi$ and $\Sigma\bar{K}$. The knowledge on these low-lying Ξ resonances is rather scarce. Several measurements are available [25–29] but not all quantum numbers and branching ratios for the different decay channels can be estimated [30]. Both resonances are too light to be accommodated in most quark models [31, 32] and, particularly for the $\Xi(1620)$ state, only the decay in the neutral $\pi\Xi$ channel has recently been observed by the Belle Collaboration [27], confirming the first experimental evidence in the same channel obtained in the 1970s [25, 26, 33]. Due to the lack of experimental data, the nature and the properties of the $\Xi(1620)$ are still open for discussion and its theoretical modeling is far away from being settled. Since this state can in principle couple to the $\Lambda-\bar{K}$ system, the possibility to access the $\Lambda\bar{K}$ interaction with the femtoscopy technique opens a new road in the study of double-strange resonances.

By considering the interaction between a Λ and a kaon, the $S = 0$ meson–baryon dynamics can be probed, in which, as for the $\Lambda-\bar{K}$ system, many inelastic channels are present (such as πN , ΣK). Effective Lagrangians describing the coupled-channel $S = 0$ system are mainly anchored to the large database on elastic πN scattering [34–37], which leads to a detailed understanding of most of the light-flavor baryonic resonances known today, such as N^* and Δ . However, there might also be states which strongly couple to inelastic channels with no net strangeness, such as ΛK [20, 38]. Providing experimental constraints on the ΛK interaction can hence contribute to improve the knowledge of the light hadronic spectrum.

Additional data on the interaction between Λ baryons and strange mesons is also important in view of the recent efforts in going beyond the non-interacting picture of hadrons in the statistical approaches applied in heavy-ion collisions (HIC) [39–41]. The proton-to-pion ratio [42], which was not properly reproduced within the basic assumption of thermal models describing the hadronic phase as a non-interacting system, found its explanation in the inclusion of the πN scattering parameters in a more sophisticated recent statistical approach [43]. Since Λ and kaons/antikaons are the most abundant strange hadrons produced in HICs, the interaction between them can be used as an input for these new calculations within the thermal model and help to shed light on the role of strangeness in the hadronization process [44].

Correlations of all the neutral and charged combinations between Λ and kaons ($\Lambda-K$, $\Lambda-\bar{K}$, $\Lambda-K_S^0$) have been published by the ALICE Collaboration in Pb–Pb collisions at a center-of-mass energy per nucleon–nucleon collision $\sqrt{s_{NN}} = 2.76$ TeV [45], and delivered the first scattering parameters on the underlying interaction, being repulsive for $\Lambda-K$ and attractive for the remaining pairs. A similar mea-

surement on $\Lambda\text{-K}_S^0$ has also been conducted recently by the CMS Collaboration in Pb–Pb collisions at $\sqrt{s_{\text{NN}}} = 5.02$ TeV [46], in which a different treatment of feed-down contributions is used.

In this Letter, we study the ΛK and $\Lambda\bar{\text{K}}$ interaction via the measurement of the correlations for the charged combinations $\Lambda\text{-K}^+ \oplus \bar{\Lambda}\text{-K}^-$ and $\Lambda\text{-K}^- \oplus \bar{\Lambda}\text{-K}^+$ in the high-multiplicity (HM) data sample in pp collisions at $\sqrt{s} = 13$ TeV [47, 48]. Note that the correlation functions of $\Lambda\text{-K}^+$ ($\Lambda\text{-K}^-$) pairs and $\bar{\Lambda}\text{-K}^-$ ($\bar{\Lambda}\text{-K}^+$) pairs are added together in order to enhance the statistical significance of the results. The results are obtained by comparing the experimental data to the modeled correlation using the Lednický–Lyuboshits analytical formula, from which scattering parameters and properties of the $\Xi(1620)$ are extracted.

2 Data analysis

The data sample studied in this work was collected by ALICE [49] at the LHC in pp collisions at $\sqrt{s} = 13$ TeV during the Run 2 period. All analyzed events passed a HM trigger, based on the measured amplitude in the V0 detector system, consisting of two arrays of plastic scintillators located at forward ($2.8 < \eta < 5.1$) and backward ($-3.7 < \eta < -1.7$) pseudorapidities [50]. The selected events correspond to the inelastic pp collisions with the top 0.17% of the measured signal amplitudes, with at least one charged particle in the range $|\eta| < 1$ (referred to as INEL > 0) [47, 48]. The resulting data sample contains events with an average of 30 produced charged particles in the pseudorapidity interval $|\eta| < 0.5$ [5]. Approximately 1.0×10^9 HM events are selected by adopting the procedure described in Refs. [4, 5, 51].

The Monte Carlo simulated data used in this analysis are obtained from the PYTHIA 8.2 event generator [52]. The transport through the ALICE detector is simulated using GEANT 3 [53] and the reconstruction follows the dedicated ALICE reconstruction algorithm [47]. An additional selection on large charged-particle multiplicities, which mimics the effect of the HM trigger, is applied.

The primary vertex (PV) of the collision is measured using the charged-particle tracks reconstructed from the Inner Tracking System (ITS) [54] and the Time Projection Chamber (TPC) [55]. A maximal displacement of the PV with respect to the nominal interaction point of 10 cm along the beam axis is required in order to ensure a uniform acceptance. Charged particles are identified using information provided by the TPC [55] and the Time-of-Flight (TOF) detector [56]. The ITS, TPC, and TOF detectors, used for charged-particle tracking and identification, cover the full azimuthal angle and the pseudorapidity interval $|\eta| < 0.9$, and are embedded in a uniform magnetic field of 0.5 T along the beam axis.

The information provided by these detectors is used to extract the kinematic and topological quantities needed to reconstruct the K ($\bar{\text{K}}$) and Λ ($\bar{\Lambda}$) candidates. The selection on these variables is varied to evaluate the related systematic uncertainties. In the following, the systematic variations of the selections specifically mentioned in the text are enclosed in parentheses.

The identification of kaons (antikaons) is conducted employing both the TPC and TOF detectors by applying a strict selection on the deviation n_σ between the measured quantities (dE/dx , time-of-flight) and the signal hypothesis for a kaon, electron, or pion, normalized by the detector resolution σ . The n_σ thresholds are chosen so as to remove possible contamination from electrons and pions to the kaon sample. The kaon candidates are selected within a transverse momentum range of $p_T \in [0.15 (0.1, 0.2), 4.0]$ GeV/ c and a pseudorapidity range of $|\eta| < 0.8 (0.75, 0.85)$, to avoid regions of the detector with limited acceptance. To significantly improve the amount of primary kaons with respect to secondary particles coming from weak decays and particle–detector interactions, a selection criterion on the Distance of Closest Approach (DCA) to the primary vertex is applied, both in the transverse plane ($\text{DCA}_{xy} < 0.1$ cm) and along the direction of the beam ($\text{DCA}_z < 0.2$ cm). The purity, referring to the fraction of correctly identified kaon and antikaon candidates, is around 99.5%.

The kinematic and topological selection criteria related to the reconstruction of Λ and $\bar{\Lambda}$, as well as the associated systematic uncertainties, are the same as described in Ref. [51]. Due to their charge neutrality and their short lifetime, the Λ candidates are reconstructed through the weak decay $\Lambda \rightarrow p\pi^-$, which has a branching ratio of $\text{BR} = (63.9 \pm 0.5)\%$ and a decay length of $c\tau = (7.89 \pm 0.06)$ cm [30]. The charge-conjugate decay is used for the $\bar{\Lambda}$ reconstruction. The candidates are then identified within a $p\pi^-$ invariant mass window of $|M_{p\pi} - M_\Lambda| < 4 \text{ MeV}/c^2$ (corresponding to about 3σ), with the nominal mass $M_\Lambda = 1116 \text{ MeV}/c^2$ [30]. This leads to purities of $P_\Lambda = 94.2\%$, $P_{\bar{\Lambda}} = 95.1\%$ for Λ and $\bar{\Lambda}$, respectively. A primary fraction of 57.6% is extracted following the procedure described in Ref. [57]. Secondary contributions from weak decays of neutral and charged Ξ baryons account for 23.2% of the candidate sample. The remaining 19.2% are attributed to Σ^0 particles.

3 Analysis of the correlation function

The observable of this analysis is the two-particle correlation function $C(k^*)$, defined as [1]

$$C(k^*) = \mathcal{N} \times \frac{N_{\text{same}}(k^*)}{N_{\text{mixed}}(k^*)}, \quad (1)$$

where $k^* = \frac{1}{2} \times |\mathbf{p}_1^* - \mathbf{p}_2^*|$ is the relative momentum of the pair in its rest frame. Here $N_{\text{same}}(k^*)$ is the k^* distribution of pairs measured in the same event, $N_{\text{mixed}}(k^*)$ is the reference distribution of uncorrelated pairs sampled from different (mixed) events. The mixed-event sample is obtained by pairing particles stemming from events with a similar number of charged particles at midrapidity and a close-by primary vertex position along the beam direction, following [4, 5, 12]. The constant \mathcal{N} is a normalization parameter determined by assuming particle pairs with large k^* to be uncorrelated, which corresponds to a flat $C(k^*) = 1$ [1]. This normalization constant \mathcal{N} is evaluated in $k^* \in [240 - 340] \text{ MeV}/c$ for $\Lambda\text{-K}^+ \oplus \bar{\Lambda}\text{-K}^-$ and in the region $[500 - 800] \text{ MeV}/c$ for $\Lambda\text{-K}^- \oplus \bar{\Lambda}\text{-K}^+$, where no resonances are present.

A total of 4.45×10^6 $\Lambda\text{-K}^+ \oplus \bar{\Lambda}\text{-K}^-$ and 4.38×10^6 $\Lambda\text{-K}^- \oplus \bar{\Lambda}\text{-K}^+$ pairs contribute to the correlation signal for $k^* < 200 \text{ MeV}/c$. For brevity, in the following $\Lambda\text{-K}^+$ denotes the combination $\Lambda\text{-K}^+ \oplus \bar{\Lambda}\text{-K}^-$ and $\Lambda\text{-K}^-$ is used for $\Lambda\text{-K}^- \oplus \bar{\Lambda}\text{-K}^+$. The resulting experimental correlation functions are shown in the upper panel of Fig. 1 and in Fig. 2.

The measured correlations are fitted with a correlation function:

$$C_{\text{tot}}(k^*) = N_D \times C_{\text{model}}(k^*) \times C_{\text{background}}(k^*), \quad (2)$$

where N_D is a normalization constant, free to vary in the fit. The default fit range is $0 < k^* < 500 \text{ MeV}/c$. A variation of $\pm 10\%$ to the upper limit of the default fit range is applied for evaluating the systematic uncertainties. The term $C_{\text{model}}(k^*) = 1 + \sum_i \lambda_i \times (C_i(k^*) - 1)$ includes the genuine correlation ($i = \text{gen}$), which arises from final state interaction among the two particles of interest, as well as residual contributions involving secondary particles from weak or electromagnetic decays and misidentified ones. Each of these contributions is weighted by the corresponding λ_i parameter, depending on the purity and on the origin of the particles [2].

The genuine contribution for $\Lambda\text{-K}^+$ and $\Lambda\text{-K}^-$ pairs amounts to $\lambda_{\text{gen}} = 51\%$; the residual correlations between kaons (antikaons) and Λ ($\bar{\Lambda}$) from the decay of Ξ ($\bar{\Xi}$) contribute each with a weight of $\lambda_{\Lambda\Xi K} = 10\%$. The correlations for the charged combinations (e.g. $\Xi^\pm\text{-K}^\pm$) are modeled with the CATS framework [58] assuming Coulomb-only interaction. The presence of a residual strong interaction between Ξ and kaons is neglected in this analysis since currently no experimental data are available and the corresponding

theoretical predictions are hence not validated yet [59, 60]. Similarly, residual correlations involving Ξ^0 and Σ^0 are considered to be flat due to the absence of Coulomb interaction. Such residual contributions, along with correlations involving misidentified particles, amount to $\lambda_{\text{flat}} = 39\%$ of the measured signal. The systematic uncertainties related to the λ_i parameters are estimated based on the purities obtained for each varied set of kinematic and topological cuts, as well as by varying the values of secondary fractions by $\pm 10\%$. In addition to the feed-down contributions, a correction for the finite experimental momentum resolution is taken into account for a direct comparison with data [2].

The last factor in Eq. 2, $C_{\text{background}}$, accounts for the non-femtoscopic background visible in both measured correlations [2]. In particular, the $\Lambda\text{-K}^+$ data are affected by the presence of the so-called mini-jet contributions, typically associated to the initial hard processes occurring at the parton level during the collision [61]. This type of background has already been observed in several meson–meson [62–65], meson–baryon [10, 12], and baryon–antibaryon femtoscopic analyses [9]. The mini-jet term included in the $C_{\text{background}}(k^*)$ for $\Lambda\text{-K}^+$ is modeled using Monte Carlo simulated data and following the same procedure adopted in Ref. [9]. A polynomial of second order is added as baseline to the mini-jet part of the background to take into account energy–momentum conservation effects developing at large k^* [2], which lead to an enhancement of the correlation function in this momentum region. The coefficients of the polynomial are fixed by a prefit of $C_{\text{background}}(k^*)$ to the $\Lambda\text{-K}^+$ data in the region of $400 < k^* < 2000$ MeV/ c . A variation of $\pm 10\%$ in the lower and upper limit of this range range is included to estimate the systematic uncertainty related to the total background. In the case of $\Lambda\text{-K}^-$, the mini-jet background is much less pronounced. The measured $\Lambda\text{-K}^-$ correlation function outside the femtoscopic region of $k^* > 200$ MeV/ c is well reproduced by Monte Carlo simulated data and no additional baselines are required to describe the large k^* region. Hence, the total $C_{\text{background}}(k^*)$ in the $\Lambda\text{-K}^-$ case is modeled using only the simulated correlation, parametrized by a third-order polynomial constrained to be flat at $k^* \rightarrow 0$ since no signal is expected to arise from the background [6, 8] at low k^* . The coefficients of the polynomial are fixed by fitting the Monte Carlo simulated data in the range $k^* \in [0, 600]$ MeV/ c , with systematic variations of the upper limit of $\pm 10\%$.

Besides the background, which shifts the data upwards with respect to unity in the region of relative momenta above 200 MeV/ c , there are several structures present in the measured $\Lambda\text{-K}^-$ correlation (upper panel in Fig. 1), related to resonances decaying into $\Lambda\text{-K}^-$ pairs. In the lower panel of Fig. 1, the invariant mass of $\Lambda\text{-K}^-$ pairs, expressed in k^* , is shown in order to better visualize the location of these three resonances. The $\Lambda\text{-K}^-$ invariant mass spectrum in k^* is obtained following the same approach employed in resonance analyses [66]. The uncorrelated mixed-event background, normalized to the signal outside the resonance region ($k^* \in [500, 800]$ MeV/ c), is subtracted from the same-event $\Lambda\text{-K}^-$ distribution, representing the raw signal. Similarly to the measured correlation function, a residual background is present which can be modeled using Monte Carlo data. The outcome of the simulations is fitted with a fourth-order polynomial and finally subtracted from the measured spectrum. The peak appearing at $k^* \approx 211$ MeV/ c (green dashed line) corresponds to the Ω baryon decaying weakly into ΛK^- with a branching ratio of $(67.8 \pm 0.7)\%$ [30]. The $\Xi(1690)$ and $\Xi(1820)$ resonances can be associated to the second and third peaks in the correlation. The negative counts in the region $100 < k^* < 200$ MeV/ c of the $\Lambda\text{-K}^-$ invariant mass are due to the presence of a residual non-resonant interaction, which will be discussed in detail in Sec. 4.

Currently the branching ratios of the strong decays of these states into ΛK^- are not precisely known [30]. In the upper x -axis of the bottom panel of Fig. 1, the corresponding mass of the resonance obtained from the kinematic relation $E = \sqrt{(k^*)^2 + m_\Lambda^2} + \sqrt{(k^*)^2 + m_K^2}$, is shown. In order to properly model the background outside the femtoscopic range, these three resonances must be taken into account. The total background correlation for $\Lambda\text{-K}^-$ can hence be written as

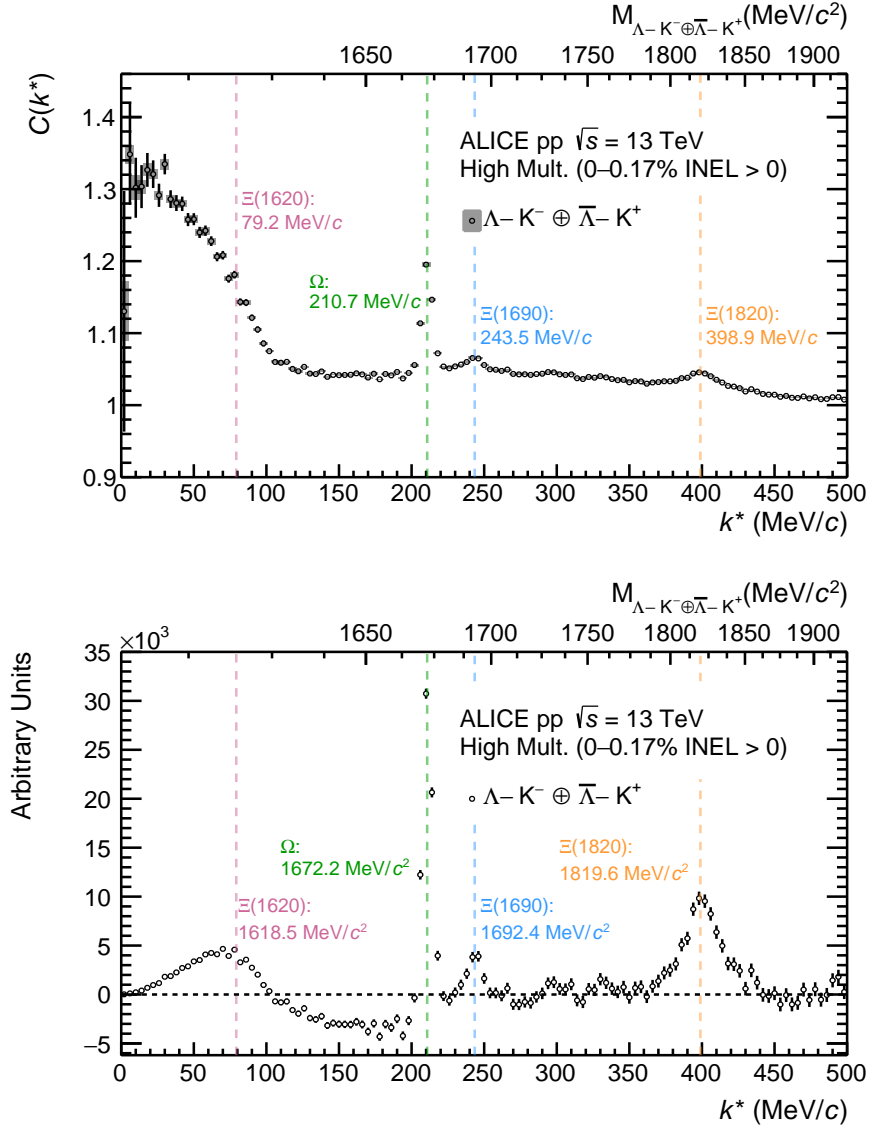


Figure 1: (Color online) Upper: measured correlation function for Λ - K^- pairs (empty points) with statistical (line) and systematic (gray boxes) uncertainties. Lower: invariant mass spectrum of Λ - K^- pairs used to build the measured correlation function. Only the statistical uncertainties are shown. The upper x -axis indicates the energy at rest $E = \sqrt{(k^*)^2 + m_\Lambda^2} + \sqrt{(k^*)^2 + m_K^2}$ of the pair written as a function of the relative momentum of the Λ - K^- pair. The colored vertical dashed lines indicate the values of the relative momentum k^* (upper panel) and the value of the energy E at rest of each resonance (lower panel) corresponding to its nominal mass extracted in the final femtoscopic fit.

$$C_{\text{background}}^{\Lambda K^-}(k^*) = \alpha_{\text{pol}3}(1 + bk^{*2} + ck^{*3}) + \alpha_\Omega f_G(M_\Omega, \sigma_\Omega) + \sum_i \alpha_i f_{\text{BW}}(M_i, \Gamma_i), \quad (3)$$

in which a Gaussian distribution f_G is used for the Ω baryon and a Breit-Wigner one f_{BW} for the two excited Ξ resonances. In order to help the convergence of the final femtoscopic fit, a fit of the total $C_{\text{background}}(k^*)$ correlation to the data is performed in the k^* region of 190 – 600 MeV/c to estimate the weights α_Ω , α_i as well as the masses and widths of the resonances. A change of $\pm 10\%$ in the upper limit of the fit range is included in the evaluation of the final systematic uncertainties. These parameters are

then kept free in the final femtoscopic fit of $C_{\text{tot}}(k^*)$ to the data and the values obtained for the masses and widths are found to be compatible with the available PDG values [30] and recent measurements [28,29]. The orange band in Figs. 2 and 3 shows the total $C_{\text{background}}(k^*)$ correlation function extracted in the final femtoscopic fit, multiplied by the normalization factor N_D , for Λ - K^+ and Λ - K^- pairs, respectively.

The last ingredient needed to model the data is the strong interaction of the Λ - K^+ and Λ - K^- pairs entering in the $C_{\text{model}}(k^*)$ in Eq. 2 via the genuine correlation function $C_{\text{gen}}(k^*)$. This is modeled for both pairs using the Lednický–Lyuboshits analytical formula [67], following the approach used in Ref. [45],

$$C(k^*)_{\text{LL}} = 1 + \left[\frac{1}{2} \left| \frac{f(k^*)}{R} \right|^2 \left(1 - \frac{d_0}{2\sqrt{\pi}R} \right) + \frac{2\Re f(k^*)}{\sqrt{\pi}R} F_1(2k^*R) - \frac{\Im f(k^*)}{R} F_2(2k^*R) \right]. \quad (4)$$

The scattering amplitude $f(k^*)$ is the quantity embedding the scattering parameters and providing information on the underlying interaction. Typically, $f(k^*)$ is expressed via the effective-range expansion (ERE) $f(k^*) = \left(\frac{1}{f_0} + \frac{1}{2}d_0k^{*2} - ik^* \right)^{-1}$, in which f_0 is the scattering length and d_0 is the effective range. The parameter R is the size of the emitting source with a Gaussian profile. In this work it was fixed using the core-resonance model taken from Ref. [51], already employed in several previous femtoscopic analyses performed in small colliding systems as pp collisions and anchored to p–p correlations. The core radius for Λ - K^+ and Λ - K^- pairs is $r_{\text{core}}(m_T) = 1.35 \text{ GeV}/c^2 = 1.11 \pm 0.04 \text{ fm}$. In order to use the core-resonance total source in Eq. 4, this must be parametrized with a Gaussian distribution. The presence of long-lived strong resonances feeding to Λ and kaons introduces a significant exponential tail for large r^* , which cannot be described with a single Gaussian [5, 6, 8, 10, 13]. The total source is hence modeled with a weighted sum of two Gaussians, leading to an effective emitting source $S_{\text{eff}}(r^*) = \lambda_S[\omega_S S_1(r^*) + (1 - \omega_S)S_2(r^*)]$, in which $r_1 = 1.202^{+0.043}_{-0.042} \text{ fm}$, $r_2 = 2.330^{+0.050}_{-0.045} \text{ fm}$, $\lambda_S = 0.9806^{+0.0006}_{-0.0008}$, and $\omega_S = 0.7993^{+0.0037}_{-0.0027}$. As systematic variation of the source function, these values are varied within the uncertainties. Due to the additive property of correlation functions, the final genuine correlation is then taken as the sum of two correlations evaluated with the two properly weighted Gaussian sources. To preserve the correct normalization of the emitting source and the unitarity of the λ parameters [2] in $C_{\text{model}}(k^*)$, a $(1 - \lambda_S)$ contribution is added.

The understanding of the ΛK^- interaction, particularly in the low k^* region, is strictly connected to the $\Xi(1620)$ state. In principle, since $\Xi(1620)$ shares the same quantum numbers as the Λ - K^- pair, the two systems can couple strongly. The Belle collaboration recently published the observation of the $\Xi(1620)$ state in the $\Xi\pi$ decay channel ($E_{\text{thr},1} = m_\pi + m_\Xi = 1461.3 \text{ MeV}/c^2$) [27]. The reported mass and widths in Ref. [27] are $M_{\Xi(1620)} = 1610.4 \pm 6.0 \text{ MeV}/c^2$, $\Gamma_{\Xi(1620)} = 60.0 \pm 4.8 \text{ MeV}$, which indicates that the decay of $\Xi(1620)$ into ΛK^- ($E_{\text{thr},2} = m_{K^-} + m_\Lambda = 1609.4 \text{ MeV}/c^2$) is kinematically allowed. No experimental evidence of this decay channel has been observed so far. The presented work provides quantitative evidence of this process.

The $\Xi(1620)$ state can be clearly seen in the peak at $k^* \approx 80 \text{ MeV}/c$ in the lower panel of Fig. 1. Hence, to model the ΛK^- interaction at low k^* , the $\Xi(1620)$ must be taken into account in the Lednický–Lyuboshits approach. Similar scenarios, with resonances contributing to the signal in the low k^* region, were observed in $K_S^0 - K^\pm$ correlations measured in pp and Pb–Pb collisions, in which the interaction mainly goes through the formation of the a_0 resonance. A way to properly include such a resonant interaction is to write the scattering amplitude in Eq. 4 in terms of the probability distribution describing the state. Due to the vicinity of the ΛK^- decay-channel threshold, the $\Xi(1620)$ resonance must be described with a Flatté-like distribution [68] such as the Sill distribution used in Ref. [69]. The corresponding scattering amplitude can be written as

$$f(k^*) = \frac{-2\tilde{\Gamma}_{\Lambda K^-}}{E^2 - M^2 + i\tilde{\Gamma}_{\Xi\pi}\sqrt{E^2 - E_{\text{thr},\Xi\pi}^2} + i\tilde{\Gamma}_{\Lambda K^-}\sqrt{E^2 - E_{\text{thr},\Lambda K^-}^2}} \quad (5)$$

in which M is the mass of the $\Xi(1620)$ state, $\tilde{\Gamma}_{i=\Xi\pi,\Lambda K^-}$ are the effective partial widths as defined in Ref. [69], and $E_{\text{thr},i=\Xi\pi,\Lambda K^-}$ are the threshold energies for the two channels, as defined above.

Besides the interaction between Λ and antikaons through the $\Xi(1620)$ state, a non-resonant strong interaction is present in the measured correlation function, which can be explicitly seen in the lower panel of Fig. 1 for $100 < k^* < 200$ MeV/ c . In this k^* region the data, corrected by the background contribution as described above, go below zero indicating a depletion in the measured Λ - K^- pairs arising from the underlying non-resonant component of the interaction. Since there are no theoretical approaches available at the moment in which the ΛK^- interaction is composed of a resonant part, through the $\Xi(1620)$ state above the ΛK^- threshold, and a non-resonant one, an effective modeling of these two contributions will be adopted employing the Lednický-Lyuboshits formula. The non-resonant $C_{\text{LL}}^{\text{non-res}}(k^*)$ and resonant $C_{\text{LL}}^{\text{res}}(k^*)$ correlations are modeled using Eq. 4: for $C_{\text{LL}}^{\text{non-res}}(k^*)$ an ERE scattering amplitude is assumed, while for $C_{\text{LL}}^{\text{res}}(k^*)$ a Sill amplitude is employed, according to Eq. 5. Taking both interactions into account, the final genuine correlation for Λ - K^- is composed of a weighted sum of a correlation including the resonant process and another one responsible for the non-resonant part

$$C_{\text{gen}}(k^*) = \omega C_{\text{LL}}^{\text{non-res}}(k^*) + (1 - \omega) C_{\text{LL}}^{\text{res}}(k^*). \quad (6)$$

The remaining free parameters to be extracted in the final femtoscopic fit of $C_{\text{tot}}(k^*)$ to the data are the weight ω for non-resonant scattering parameters ($\Re f_0, \Im f_0, d_0$), the mass M , the partial widths $\tilde{\Gamma}_{i=1,2}$ of the $\Xi(1620)$ state, and the masses and widths of the Ω , $\Xi(1690)$, and $\Xi(1820)$.

4 Results

The results for Λ - K^+ and Λ - K^- systems are shown in Figs. 2 and 3, respectively. The lower panels in each plot show the deviation between data and model in terms of number of standard deviations n_σ . The width of the band represents the total uncertainty of the fit, including the statistical and the systematic uncertainties. The gray boxes correspond to the systematic uncertainties of the data and they maximally amount to 3%–4% in the lowest k^* interval for each pair. The measured Λ - K^+ correlation function, shown in Fig. 2, is below unity at low k^* , indicating a repulsive strong interaction between Λ and kaons, in agreement with the femtoscopic results obtained in Pb–Pb collisions [45]. The behavior of the data is well reproduced by the fit using Eq. 2 with an average reduced χ^2/NDF of 3.9 estimated in the default fit range.

In Fig. 3, the results for the Λ - K^- system are presented. The light cyan band represents the total correlation function (Eq. 2) with the genuine interaction modeled, including a non-resonant and a resonant contribution through the formation of the $\Xi(1620)$. The fit well describes the data and the reduced χ^2/NDF , evaluated within the fit range, is 2.9. The obtained weight ω in Eq. 6 is found to be $0.950 \pm 0.005(\text{stat.}) \pm 0.006(\text{syst.})$, indicating that a dominant contribution from the non-resonant interaction is needed to reproduce the data. However, the approach taking into account both contributions, which is used in this work, should be considered as a phenomenological approach and more theoretical investigations are needed in order to provide a better description of the interplay between resonant and non-resonant processes. The two additional bands reported in Fig. 3 correspond to the weighted correlation functions obtained from the fit, which represent the resonant (violet) and non-resonant (olive) ΛK^- interaction, respectively.

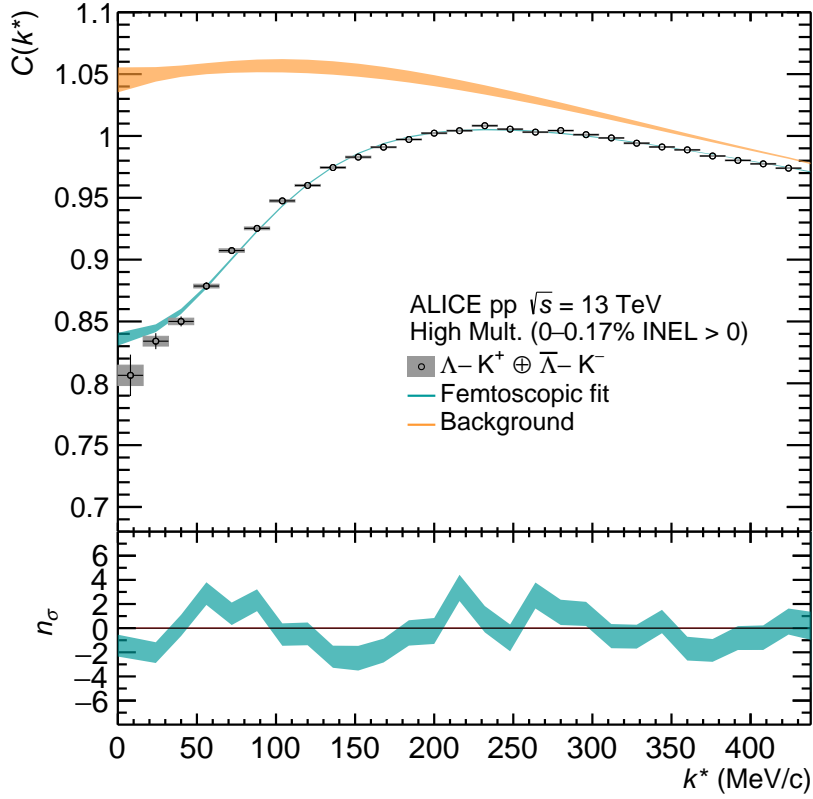


Figure 2: (Color online) Measured correlation function of Λ - K^+ pairs. Statistical (bars) and systematic (boxes) uncertainties are shown separately. The light cyan band represents the total fit obtained using Eq. 2 from which the normalization N_D , and the scattering parameters ($\Re f_0, \Im f_0$, and d_0) are extracted. The orange band represents the $C_{\text{background}}(k^*)$ contribution, modeled as described in Section 3, and multiplied by the constant N_D . Lower panel: n_σ deviation between data and model in terms of numbers of standard deviations.

The Λ - K^- pairs interacting through the resonance lead to a rather flat correlation profile at low k^* , which peaks at the mass of the observed $\Xi(1620)$ ($k^* \approx 80$ MeV/c) and then quickly reaches unity. The extracted values of mass and partial effective widths for the $\Xi(1620)$ from the femtosopic fit are also reported in Fig. 3. The mass $M_{\Xi(1620)} = 1618.49 \pm 0.28(\text{stat.}) \pm 0.21(\text{syst.})$ MeV/ c^2 obtained from the fit, as stated in Sec. 3, is in agreement with the Belle measurement [27]. Due to the vicinity of the ΛK^- threshold, the numerical values of $\tilde{\Gamma}_{\Xi\pi} = 1.01 \pm 0.14(\text{stat.}) \pm 0.39(\text{syst.})$ MeV and $\tilde{\Gamma}_{\Lambda K^-} = 115.99 \pm 8.56(\text{stat.}) \pm 4.08(\text{syst.})$ MeV, obtained from the fit using a Flatté-like distribution, might not provide the correct quantitative results [70], however the large $\tilde{\Gamma}_{\Lambda K^-}$ indicates a strong coupling of the $\Xi(1620)$ state to the ΛK^- channel. To provide a qualitative comparison between the results obtained in this work and the total width reported by Belle, the determination of the poles for the Sill scattering amplitude in Eq. 5 is performed. By inserting the values of the extracted mass and widths in the denominator and searching for its zeros, the pole position for the $\Xi(1620)$ resonance corresponds to a state with a mass $M = 1616.34^{+0.01}_{-0.05}$ MeV/ c^2 and a total width of $\Gamma = 12.00 \pm 1.24$ MeV. The total uncertainty reported is propagated in the calculation from the quadratic sum of the statistical and systematic error on the mass and widths obtained from the femtosopic fit. The value of the mass obtained from the pole is compatible with the results reported by Belle, while the width Γ is smaller. This discrepancy can arise since, as mentioned above, the presence of a close-by threshold strongly influences the extracted properties of the resonance and the typical interpretation of the mass and in particular of the width obtained directly from the energy of the pole might not hold for a near-threshold resonance, as the $\Xi(1620)$ in this case.

The ERE of the scattering amplitude $f(k^*)$ in the Lednický-Lyuboshits formula allows the scattering pa-

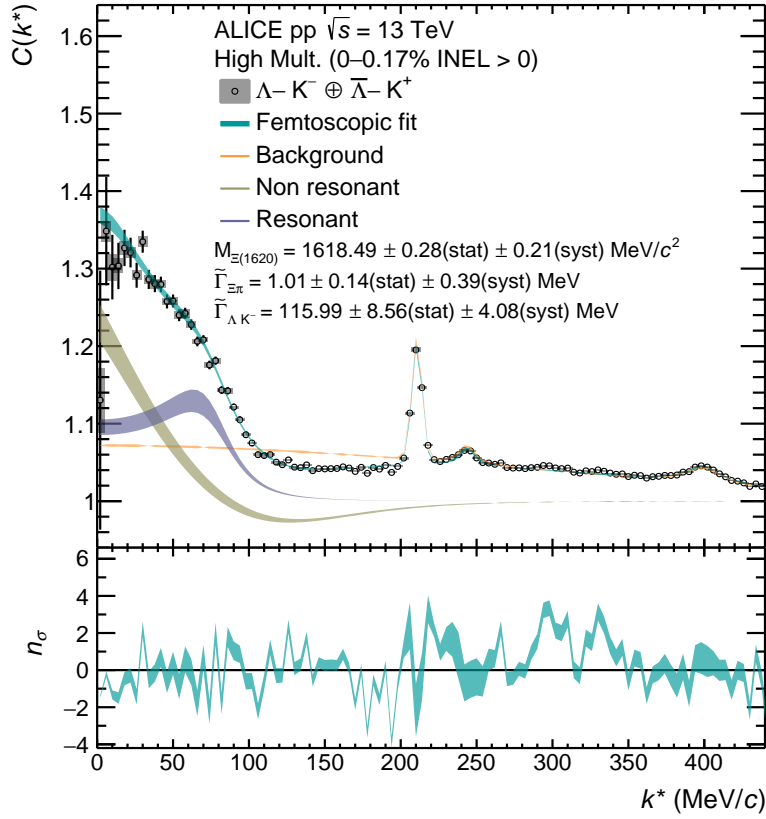


Figure 3: (Color online) Measured correlation function of Λ - K^- pairs. Statistical (bars) and systematic (boxes) uncertainties are shown separately. The light cyan band represents the total fit obtained using Eq. 2 from which the normalization N_D , the non-resonant scattering parameters ($\Re f_0, \Im f_0$ and d_0) and the properties of the $\Xi(1620)$ state are extracted. The violet band represents the $C_{LL}^{\text{res}}(k^*)$ correlation multiplied by the corresponding weight $(1 - \omega)$, while the olive green band is the $\omega C_{LL}^{\text{non-res}}(k^*)$. The orange band represents the $C_{\text{background}}(k^*)$ modeled using the Monte Carlo simulations multiplied by the constant N_D . Lower panel: n_σ deviation between data and model in terms of numbers of standard deviations.

rameters $\Re f_0$, $\Im f_0$, and d_0 to be extracted. The results for ΛK^+ (red diamonds) and for the non-resonant ΛK^- interaction (red circles) are shown in Fig. 4 with statistical (bars) and systematic (shaded areas) uncertainties, and summarized in Table 1. The left panel of Fig. 4 shows the real part of the scattering length $\Re f_0$ (x -axis) as a function of the imaginary part $\Im f_0$ (y -axis) obtained in this work and its comparison to the measurements in Pb–Pb collisions (blue markers) [45]. The available theoretical predictions for $\Re f_0$ and $\Im f_0$, also presented in Fig. 4, are based on unitarized chiral perturbation theory at leading order (LO) (green open circles [18], light-cyan open circles [22]) and on the standard chiral perturbation theory at next-to-leading order (NLO) (orange open squares [34], magenta open markers [35]). The output of these chiral calculations strongly depends on the so-called low-energy and subtraction constants, parameters of the model which need as input the experimental data to be fixed. In particular, the results obtained in Ref. [34, 35] arise from a full treatment of the $SU(3)$ flavor meson–baryon interaction and are hence anchored to large $|S| = 0$ pion–nucleon database. Moreover, to reduce the number of input parameters, isospin symmetry is assumed, and then the crossing symmetry leads to almost identical scattering parameters for the ΛK^+ and ΛK^- interaction. In the unitarized framework of [18, 22], the $\Xi(1620)$ is dynamically generated, meaning that the state is not introduced in the Lagrangian investigated at LO, but it appears in the scattering amplitude due to the meson–baryon interaction dynamics. The results in Ref. [18] were published before the Belle measurement on $\Xi(1620)$ [27], hence the model parameters were constrained mainly by symmetry assumptions and by experimental data on the antikaon–nucleon

interaction. The scattering amplitude obtained within this work has been studied in Ref. [22], allowing for variations in the subtraction constants of the model in order to reproduce the $\Xi(1620)$ properties measured by Belle. An agreement with the measured $\Xi(1620)$ mass and width is achieved only with very large values of these constants, in contrast with the typical trend seen in similar works. Such discrepancy might arise from the inclusion of only LO contributions in the interaction and it can be investigated in the future with an updated version of the chiral potentials in Ref. [71] at NLO that recently became available. The studies in Ref. [18, 22] show that the ΛK^- interaction is crucial in the understanding of the $\Xi(1620)$ state and it must be properly taken into account in the dynamics.

The negative value of $\Re f_0$ obtained in this work for $\Lambda-K^+$ pairs is compatible with the Pb–Pb results [45], confirming the presence of a repulsive interaction. This is in tension with the chiral calculations [34, 35], indicating an overall attraction. The extracted $\Lambda K^+ \Im f_0$ is in agreement within 1σ with the value obtained from the Pb–Pb measurements and it is in line with the available predictions. The non-negligible value (roughly $1/3$ of the $\Re f_0$), reported in Table 1, indicates the presence of inelastic channels in the measured interaction. The d_0 is shown in the right panel of Fig. 4 and it can be seen that, for both $\Lambda-K^+$ and $\Lambda-K^-$ systems, the values extracted in pp and Pb–Pb colliding systems are in agreement within uncertainties.

The $\Lambda-K^-$ pairs undergoing the non-resonant interaction in Fig. 3 (olive green bands) show an attractive interaction with a depletion in the region $100 < k^* < 200$ MeV/ c (as seen in the lower panel of Fig. 1) given by a non-negligible $\Im f_0$. The $\Re f_0$ lies in the positive side of the x -axis, hence indicating an attractive ΛK^- strong interaction as observed in Pb–Pb collisions. Similarly, the $\Im f_0$ is compatible within uncertainties with Pb–Pb results. The agreement between the non-resonant ΛK^- scattering parameters obtained in this work and the ones obtained in Pb–Pb collisions is expected since in large colliding systems the effect of resonances, such as the $\Xi(1620)$, on the measured correlation function is suppressed. Hence, the femtoscopic signal will be driven by the non-resonant contribution. The theoretical models currently available on the ΛK^- interaction are far from converging to a common description of this system, as can be seen in the predicted values of scattering parameters in Fig. 4. As mentioned above, the tension mainly arises from the extremely scarce amount of data available on this system. The work presented in this Letter will significantly improve the knowledge on the interactions between Λ and antikaons and shed light on the role played by the $\Xi(1620)$ state, observed for the first time in this decay channel.

Table 1: Extracted scattering parameters for ΛK^+ interaction and for the non-resonant part of ΛK^- interaction in pp collisions. Statistical and systematic uncertainties are reported.

Pair	$\Lambda-K^+$	$\Lambda-K^-$
$\Re f_0$ (fm)	$-0.61 \pm 0.03(\text{stat}) \pm 0.03(\text{syst})$	$0.33 \pm 0.03(\text{stat}) \pm 0.02(\text{syst})$
$\Im f_0$ (fm)	$0.23 \pm 0.06(\text{stat}) \pm 0.04(\text{syst})$	$0.46 \pm 0.03(\text{stat}) \pm 0.02(\text{syst})$
d_0 (fm)	$0.80 \pm 0.19(\text{stat}) \pm 0.18(\text{syst})$	$-5.47 \pm 0.36(\text{stat}) \pm 0.26(\text{syst})$

5 Summary

The two-particle correlation technique is used to access the strong interaction between Λ hyperons and charged kaons. This is achieved by measuring the $\Lambda-K^+$ and $\Lambda-K^-$ correlation functions in pp collisions, down to zero momenta. The results presented in this work provide the most precise data on these interactions. The ΛK^+ interaction is found to be repulsive, with a non-negligible $\Im f_0$, indicating that inelastic channels are present. The measured $\Lambda-K^-$ correlation function shows a signal above unity at low k^* , pointing to an overall attractive interaction, as well as several resonances at different k^* values above 200 MeV/ c . The masses and widths of these states, extracted from the fit to the correlation function, are

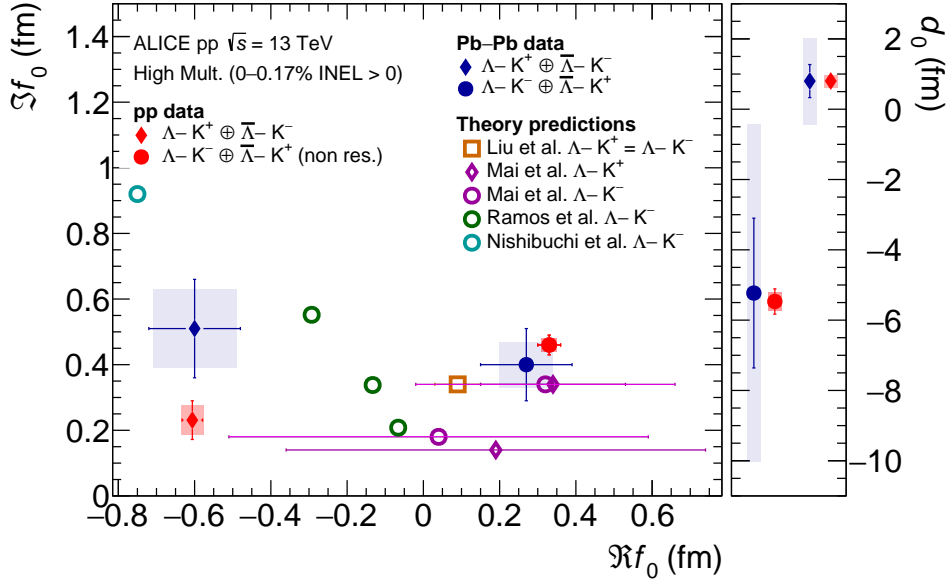


Figure 4: (Color online) Left: extracted $\Re f_0$ and $\Im f_0$ for the ΛK^+ (red diamonds) and ΛK^- (red dots) interaction in pp collisions, compared to Pb–Pb results (blue) [45] and available models (orange [34], magenta [35], green [18], and light cyan [22]). For [18], the scattering parameters obtained for different sets of input parameters are reported. Statistical (bars) and systematic (boxes) uncertainties are shown. Right: extracted effective range d_0 obtained in this work (red) and in Pb–Pb collisions (blue) [45].

compatible with the Ω baryon and with two excited Ξ states: the $\Xi(1690)$ and the $\Xi(1820)$. The invariant mass spectrum of the $\Lambda-K^-$ pairs, obtained from the same- and mixed-event distributions entering the measured correlation function shows an additional peak at $k^* \approx 80$ MeV/ c . This structure corresponds to the $\Xi(1620)$ state, expected to couple to the $\Lambda-K^-$ system. The $\Xi(1620)$ is observed so far only in the $\Xi\pi$ channel [25–27], hence these data represent the first experimental evidence of the decay of the $\Xi(1620)$ into $\Lambda-K^-$ pairs. The measurements performed in this work show that the $\Xi(1620)$ plays an important role at the level of the strong ΛK^- interaction. To reproduce the measured $\Lambda-K^-$ correlation two contributions must be taken into account in the genuine interaction: a resonant term, in which $\Lambda-K^-$ pairs interact through the formation of $\Xi(1620)$ and modeled via a Sill distribution [69], and a residual non-resonant part. Both contributions are modeled using the Lednický–Lyuboshits analytical formula with different scattering amplitudes $f(k^*)$. The extracted mass and partial widths for the $\Xi(1620)$ state are expressed in terms of poles of the Sill scattering amplitude. The mass is found to be consistent with the recent Belle measurements in the $\Xi\pi$ decay channel. The extracted scattering parameters for the ΛK^+ and the ΛK^- (non-resonant) interaction are in agreement with the femtoscopic measurements of the same pairs performed by the ALICE collaboration in Pb–Pb collisions.

The presented data provide important experimental constraints for low-energy effective theories, aiming at describing the strangeness $S = 0$ and $S = -2$ sectors of the meson–baryon interaction, and show the possibility to investigate the role of still not established resonances, such as the $\Xi(1620)$, in hadron–hadron interactions.

Acknowledgements

The ALICE Collaboration is grateful to Prof. Francesco Giacosa for the extremely valuable guidance on the theoretical aspects and to Dr. Albert Feijoo for the fruitful discussions.

The ALICE Collaboration would like to thank all its engineers and technicians for their invaluable con-

tributions to the construction of the experiment and the CERN accelerator teams for the outstanding performance of the LHC complex. The ALICE Collaboration gratefully acknowledges the resources and support provided by all Grid centres and the Worldwide LHC Computing Grid (WLCG) collaboration. The ALICE Collaboration acknowledges the following funding agencies for their support in building and running the ALICE detector: A. I. Alikhanyan National Science Laboratory (Yerevan Physics Institute) Foundation (ANSL), State Committee of Science and World Federation of Scientists (WFS), Armenia; Austrian Academy of Sciences, Austrian Science Fund (FWF): [M 2467-N36] and Nationalstiftung für Forschung, Technologie und Entwicklung, Austria; Ministry of Communications and High Technologies, National Nuclear Research Center, Azerbaijan; Conselho Nacional de Desenvolvimento Científico e Tecnológico (CNPq), Financiadora de Estudos e Projetos (Finep), Fundação de Amparo à Pesquisa do Estado de São Paulo (FAPESP) and Universidade Federal do Rio Grande do Sul (UFRGS), Brazil; Bulgarian Ministry of Education and Science, within the National Roadmap for Research Infrastructures 2020;2027 (object CERN), Bulgaria; Ministry of Education of China (MOEC) , Ministry of Science & Technology of China (MSTC) and National Natural Science Foundation of China (NSFC), China; Ministry of Science and Education and Croatian Science Foundation, Croatia; Centro de Aplicaciones Tecnológicas y Desarrollo Nuclear (CEADEN), Cubaenergía, Cuba; Ministry of Education, Youth and Sports of the Czech Republic, Czech Republic; The Danish Council for Independent Research | Natural Sciences, the VILLUM FONDEN and Danish National Research Foundation (DNRF), Denmark; Helsinki Institute of Physics (HIP), Finland; Commissariat à l’Energie Atomique (CEA) and Institut National de Physique Nucléaire et de Physique des Particules (IN2P3) and Centre National de la Recherche Scientifique (CNRS), France; Bundesministerium für Bildung und Forschung (BMBF) and GSI Helmholtzzentrum für Schwerionenforschung GmbH, Germany; General Secretariat for Research and Technology, Ministry of Education, Research and Religions, Greece; National Research, Development and Innovation Office, Hungary; Department of Atomic Energy Government of India (DAE), Department of Science and Technology, Government of India (DST), University Grants Commission, Government of India (UGC) and Council of Scientific and Industrial Research (CSIR), India; National Research and Innovation Agency - BRIN, Indonesia; Istituto Nazionale di Fisica Nucleare (INFN), Italy; Japanese Ministry of Education, Culture, Sports, Science and Technology (MEXT) and Japan Society for the Promotion of Science (JSPS) KAKENHI, Japan; Consejo Nacional de Ciencia (CONACYT) y Tecnología, through Fondo de Cooperación Internacional en Ciencia y Tecnología (FONCICYT) and Dirección General de Asuntos del Personal Académico (DGAPA), Mexico; Nederlandse Organisatie voor Wetenschappelijk Onderzoek (NWO), Netherlands; The Research Council of Norway, Norway; Commission on Science and Technology for Sustainable Development in the South (COMSATS), Pakistan; Pontificia Universidad Católica del Perú, Peru; Ministry of Education and Science, National Science Centre and WUT ID-UB, Poland; Korea Institute of Science and Technology Information and National Research Foundation of Korea (NRF), Republic of Korea; Ministry of Education and Scientific Research, Institute of Atomic Physics, Ministry of Research and Innovation and Institute of Atomic Physics and University Politehnica of Bucharest, Romania; Ministry of Education, Science, Research and Sport of the Slovak Republic, Slovakia; National Research Foundation of South Africa, South Africa; Swedish Research Council (VR) and Knut & Alice Wallenberg Foundation (KAW), Sweden; European Organization for Nuclear Research, Switzerland; Suranaree University of Technology (SUT), National Science and Technology Development Agency (NSTDA), Thailand Science Research and Innovation (TSRI) and National Science, Research and Innovation Fund (NSRF), Thailand; Turkish Energy, Nuclear and Mineral Research Agency (TENMAK), Turkey; National Academy of Sciences of Ukraine, Ukraine; Science and Technology Facilities Council (STFC), United Kingdom; National Science Foundation of the United States of America (NSF) and United States Department of Energy, Office of Nuclear Physics (DOE NP), United States of America. In addition, individual groups or members have received support from: European Research Council, Strong 2020 - Horizon 2020 (grant nos. 950692, 824093), European Union; Academy of Finland (Center of Excellence in Quark Matter) (grant nos. 346327, 346328), Finland.

References

- [1] M. A. Lisa, S. Pratt, R. Soltz, and U. Wiedemann, “Femtoscopy in relativistic heavy ion collisions”, *Ann. Rev. Nucl. Part. Sci.* **55** (2005) 357–402, arXiv:nucl-ex/0505014.
- [2] ALICE Collaboration, S. Acharya *et al.*, “p-p, p- Λ and Λ - Λ correlations studied via femtoscopy in pp reactions at $\sqrt{s} = 7$ TeV”, *Phys. Rev.* **C99** (2019) 024001, arXiv:1805.12455 [nucl-ex].
- [3] ALICE Collaboration, S. Acharya *et al.*, “First Observation of an Attractive Interaction between a Proton and a Cascade Baryon”, *Phys. Rev. Lett.* **123** (2019) 112002, arXiv:1904.12198 [nucl-ex].
- [4] ALICE Collaboration, S. Acharya *et al.*, “Investigation of the p- Σ^0 interaction via femtoscopy in pp collisions”, *Phys. Lett. B* **805** (2020) 135419, arXiv:1910.14407 [nucl-ex].
- [5] ALICE Collaboration, S. Acharya *et al.*, “Unveiling the strong interaction among hadrons at the LHC”, *Nature* **588** (2020) 232–238, arXiv:2005.11495 [nucl-ex].
- [6] ALICE Collaboration, S. Acharya *et al.*, “Exploring the Λ - Σ coupled system with high precision correlation techniques at the LHC”, *Phys. Lett. B* **833** (2022) 137272, arXiv:2104.04427 [nucl-ex].
- [7] ALICE Collaboration, S. Acharya *et al.*, “Study of the Λ - Λ interaction with femtoscopy correlations in pp and p-Pb collisions at the LHC”, *Phys. Lett. B* **797** (2019) 134822, arXiv:1905.07209 [nucl-ex].
- [8] ALICE Collaboration, S. Acharya *et al.*, “First measurement of the Λ - Ξ interaction in proton-proton collisions at the LHC”, *Phys. Lett. B* (2022) 137223. <https://www.sciencedirect.com/science/article/pii/S0370269322003574>.
- [9] ALICE Collaboration, S. Acharya *et al.*, “Investigating the role of strangeness in baryon-antibaryon annihilation at the LHC”, *Phys. Lett. B* **829** (2022) 137060, arXiv:2105.05190 [nucl-ex].
- [10] ALICE Collaboration, S. Acharya *et al.*, “Experimental Evidence for an Attractive p- ϕ Interaction”, *Phys. Rev. Lett.* **127** (2021) 172301, arXiv:2105.05578 [nucl-ex].
- [11] ALICE Collaboration, S. Acharya *et al.*, “First study of the two-body scattering involving charm hadrons”, *Phys. Rev. D* **106** (2022) 052010, arXiv:2201.05352 [nucl-ex].
- [12] ALICE Collaboration, S. Acharya *et al.*, “Scattering studies with low-energy kaon-proton femtoscopy in proton-proton collisions at the LHC”, *Phys. Rev. Lett.* **124** (2020) 092301, arXiv:1905.13470 [nucl-ex].
- [13] ALICE Collaboration, S. Acharya *et al.*, “Constraining the $\bar{K}N$ coupled channel dynamics using femtoscopic correlations at the LHC”, *Eur.Phys.J.C* **83** (5, 2022), arXiv:2205.15176 [nucl-ex].
- [14] ALICE Collaboration, S. Acharya *et al.*, “Kaon-proton strong interaction at low relative momentum via femtoscopy in Pb-Pb collisions at the LHC”, *Phys. Lett. B* **822** (2021) 136708, arXiv:2105.05683 [nucl-ex].
- [15] M. Jonathan *et al.*, “Lattice QCD evidence that the $\Lambda(1405)$ resonance is an antikaon-nucleon molecule”, *Phys. Rev. Lett.* **114** (2015) 132002, arXiv:1411.3402 [hep-lat].
- [16] Y. Kamiya and T. Hyodo, “Structure of near-threshold quasibound states”, *Phys. Rev. C* **93** (2016) 035203, arXiv:1509.00146 [hep-ph].
- [17] Y. Kamiya and T. Hyodo, “Generalized weak-binding relations of compositeness in effective field theory”, *PTEP* **2017** (2017) 023D02, arXiv:1607.01899 [hep-ph].
- [18] A. Ramos, E. Oset, and C. Bennhold, “On the spin, parity and nature of the $\Xi(1620)$ resonance”, *Phys. Rev. Lett.* **89** (2002) 252001, arXiv:nucl-th/0204044.
- [19] C. Garcia-Recio, M. F. M. Lutz, and J. Nieves, “Quark mass dependence of s wave baryon resonances”, *Phys. Lett. B* **582** (2004) 49–54, arXiv:nucl-th/0305100.

- [20] T. Sekihara, T. Arai, J. Yamagata-Sekihara, and S. Yasui, “Compositeness of baryonic resonances: Application to the $\Delta(1232)$, $N(1535)$, and $N(1650)$ resonances”, *Phys. Rev. C* **93** (2016) 035204, arXiv:1511.01200 [hep-ph].
- [21] K. Miyahara, T. Hyodo, M. Oka, J. Nieves, and E. Oset, “Theoretical study of the $\Xi(1620)$ and $\Xi(1690)$ resonances in $\Xi_c \rightarrow \pi + MB$ decays”, *Phys. Rev. C* **95** (2017) 035212, arXiv:1609.00895 [nucl-th].
- [22] T. Nishibuchi and T. Hyodo, “Nature of excited Ξ baryons with threshold effects”, in *14th International Conference on Hypernuclear and Strange Particle Physics*. 8, 2022. arXiv:2208.14608 [hep-ph].
- [23] Z.-Y. Wang, J.-J. Qi, J. Xu, and X.-H. Guo, “Analyzing $\Xi(1620)$ in the molecule picture in the Bethe-Salpeter equation approach”, *Eur. Phys. J. C* **79** (2019) 640, arXiv:1901.04474 [hep-ph].
- [24] K. Chen, R. Chen, Z.-F. Sun, and X. Liu, “ $\bar{K}\Lambda$ molecular explanation to the newly observed $\Xi(1620)^0$ ”, *Phys. Rev. D* **100** (2019) 074006, arXiv:1906.05553 [hep-ph].
- [25] R. T. Ross, T. Buran, J. L. Lloyd, J. H. Mulvey, and D. Radojicic, “ $\Xi \pi$ resonance with mass 1606 MeV/c²”, *Phys. Lett. B* **38** (1972) 177–180.
- [26] E. Briefel *et al.*, “Search for Ξ^* Production in K-p Interactions at 2.87 GeV/c”, *Phys. Rev. D* **16** (1977) 2706.
- [27] Belle Collaboration, M. Sumihama *et al.*, “Observation of $\Xi(1620)^0$ and evidence for $\Xi(1690)^0$ in $\Xi_c^+ \rightarrow \Xi^- \pi^+ \pi^+$ decays”, *Phys. Rev. Lett.* **122** (2019) 072501, arXiv:1810.06181 [hep-ex].
- [28] BESIII Collaboration, M. Ablikim *et al.*, “Measurement of the cross section for $e^+e^- \rightarrow \Xi^- \bar{\Xi}^+$ and observation of an excited Ξ baryon”, *Phys. Rev. Lett.* **124** (2020) 032002, arXiv:1910.04921 [hep-ex].
- [29] LHCb Collaboration, R. Aaij *et al.*, “Evidence of a $J/\psi\Lambda$ structure and observation of excited Ξ^- states in the $\Xi_b^- \rightarrow J/\psi\Lambda K^-$ decay”, *Sci. Bull.* **66** (2021) 1278–1287, arXiv:2012.10380 [hep-ex].
- [30] Particle Data Group Collaboration, R. L. Workman *et al.*, “Review of Particle Physics”, *PTEP* **2022** (2022) 083C01.
- [31] S. Capstick and N. Isgur, “Baryons in a relativized quark model with chromodynamics”, *Phys. Rev. D* **34** (1986) 2809–2835.
- [32] W. H. Blask, U. Bohn, M. G. Huber, B. C. Metsch, and H. R. Petry, “Hadron spectroscopy with instanton induced quark forces”, *Z. Phys. A* **337** (1990) 327–335.
- [33] A. d. Bellefon, A. Berthon, and P. Billoir, “Reactions $K^- p \rightarrow \Xi^- K^0 \pi^0$ between 2210 and 2435 MeV c.m.s energy”, *Nuovo Cim. A* **28** (1975) 289.
- [34] Y.-R. Liu and S.-L. Zhu, “Meson-baryon scattering lengths in HB χ PT”, *Phys. Rev. D* **75** (2007) 034003, arXiv:hep-ph/0607100.
- [35] M. Mai, P. C. Bruns, B. Kubis, and U.-G. Meissner, “Aspects of meson-baryon scattering in three and two-flavor chiral perturbation theory”, *Phys. Rev. D* **80** (2009) 094006, arXiv:0905.2810 [hep-ph].
- [36] D. Ronchen *et al.*, “Coupled-channel dynamics in the reactions $\pi N \rightarrow \pi N, \eta N, K\Lambda, K\Sigma$ ”, *Eur. Phys. J. A* **49** (2013) 44, arXiv:1211.6998 [nucl-th].
- [37] Y.-F. Wang, D. Rönchen, U.-G. Meißner, Y. Lu, C.-W. Shen, and J.-J. Wu, “Reaction $\pi N \rightarrow \omega N$ in a dynamical coupled-channel approach”, *Phys. Rev. D* **106** (2022) 094031, arXiv:2208.03061 [nucl-th].
- [38] P. C. Bruns, M. Mai, and U. G. Meissner, “Chiral dynamics of the S11(1535) and S11(1650) resonances revisited”, *Phys. Lett. B* **697** (2011) 254–259, arXiv:1012.2233 [nucl-th].
- [39] R. Dashen, S.-K. Ma, and H. J. Bernstein, “S Matrix formulation of statistical mechanics”, *Phys.*

- Rev.* **187** (1969) 345–370.
- [40] P. M. Lo, “S-matrix formulation of thermodynamics with N-body scatterings”, *Eur. Phys. J. C* **77** (2017) 533, arXiv:1707.04490 [hep-ph].
- [41] R. Venugopalan and M. Prakash, “Thermal properties of interacting hadrons”, *Nucl. Phys. A* **546** (1992) 718–760.
- [42] ALICE Collaboration, B. Abelev *et al.*, “Centrality dependence of π , K, p production in Pb–Pb collisions at $\sqrt{s_{\text{NN}}} = 2.76$ TeV”, *Phys. Rev. C* **88** (2013) 044910, arXiv:1303.0737 [hep-ex].
- [43] A. Andronic, P. Braun-Munzinger, B. Friman, P. M. Lo, K. Redlich, and J. Stachel, “The thermal proton yield anomaly in Pb-Pb collisions at the LHC and its resolution”, *Phys. Lett. B* **792** (2019) 304–309, arXiv:1808.03102 [hep-ph].
- [44] ALICE Collaboration, J. Adam *et al.*, “Enhanced production of multi-strange hadrons in high-multiplicity proton-proton collisions”, *Nature Phys.* **13** (2017) 535–539, arXiv:1606.07424 [nucl-ex].
- [45] ALICE Collaboration, S. Acharya *et al.*, “ Λ K femtoscopy in Pb–Pb collisions at $\sqrt{s_{\text{NN}}} = 2.76$ TeV”, *Phys. Rev. C* **103** (2021) 055201, arXiv:2005.11124 [nucl-ex].
- [46] CMS Collaboration, “ K_S^0 and $\Lambda(\bar{\Lambda})$ two-particle femtoscopic correlations in PbPb collisions at $\sqrt{s_{\text{NN}}} = 5.02$ TeV”, arXiv:2301.05290 [nucl-ex].
- [47] ALICE Collaboration, K. Aamodt *et al.*, “The ALICE experiment at the CERN LHC”, *J. Instr.* **3** (2008) S08002.
- [48] ALICE Collaboration, B. Abelev *et al.*, “Performance of the ALICE experiment at the CERN LHC”, *Int. J. Mod. Phys. A* **29** (2014) 1430044, arXiv:1402.4476 [nucl-ex].
- [49] ALICE Collaboration, “The ALICE experiment – A journey through QCD”, arXiv:2211.04384 [nucl-ex].
- [50] ALICE Collaboration, E. Abbas *et al.*, “Performance of the ALICE VZERO system”, *J. Instrum.* **8** (2013) P10016–P10016, arXiv:1306.3130 [nucl-ex].
- [51] ALICE Collaboration, S. Acharya *et al.*, “Search for a common baryon source in high-multiplicity pp collisions at the LHC”, *Phys. Lett. B* **811** (2020) 135849, arXiv:2004.08018 [nucl-ex].
- [52] T. Sjöstrand *et al.*, “An Introduction to PYTHIA 8.2”, *Comput. Phys. Commun.* **191** (2015) 159–177, arXiv:1410.3012 [hep-ph].
- [53] R. Brun, A. McPherson, P. Zancarini, M. Maire, and F. Bruyant, “Geant 3: user’s guide geant 3.10, geant 3.11”, tech. rep., CERN, 1987.
- [54] ALICE Collaboration, K. Aamodt *et al.*, “Alignment of the ALICE Inner Tracking System with cosmic-ray tracks”, *JINST* **5** (2010) P03003, arXiv:1001.0502 [physics.ins-det].
- [55] J. Alme, Y. Andres, H. Appelshäuser, S. Bablok, N. Bialas, *et al.*, “The ALICE TPC, a large 3-dimensional tracking device with fast readout for ultra-high multiplicity events”, *Nucl.Instrum.Meth. A* **622** (2010) 316–367, arXiv:1001.1950 [physics.ins-det].
- [56] A. Akindinov *et al.*, “Performance of the ALICE Time-Of-Flight detector at the LHC”, *Eur. Phys. J. Plus* **128** (2013) 44.
- [57] ALICE Collaboration, S. Acharya *et al.*, “Exploring the $\text{NA}-\text{N}\Sigma$ coupled system with high precision correlation techniques at the LHC”, *Phys. Lett. B* **833** (2022) 137272, arXiv:2104.04427 [nucl-ex].
- [58] D. Mihaylov, V. Mantovani Sarti, O. Arnold, L. Fabbietti, B. Hohlweger, and A. Mathis, “A femtoscopic Correlation Analysis Tool using the Schrödinger equation (CATS)”, *Eur. Phys. J. C* **78** (2018) 394, arXiv:1802.08481 [hep-ph].
- [59] W. L. Wang, F. Huang, Z. Y. Zhang, and F. Liu, “ Ξ anti-K interaction in a chiral model”, *J. Phys. G* **35** (2008) 085003.
- [60] M. G. L. Nogueira-Santos and C. C. Barros, “Low energy kaon- Ξ interaction in an effective chiral










- model”, *Phys. Rev. C* **102** (2020) 055205.
- [61] ALICE Collaboration, J. Adam *et al.*, “Insight into particle production mechanisms via angular correlations of identified particles in pp collisions at $\sqrt{s} = 7$ TeV”, *Eur. Phys. J. C* **77** (2017) 569, arXiv:1612.08975 [nucl-ex]. [Erratum: *Eur. Phys. J. C* **79** no.12(2019)].
- [62] ALICE Collaboration, B. Abelev *et al.*, “ $K_S^0 - K_S^0$ correlations in pp collisions at $\sqrt{s} = 7$ TeV from the LHC ALICE experiment”, *Phys. Lett. B* **717** (2012) 151–161, arXiv:1206.2056 [hep-ex].
- [63] ALICE Collaboration, B. Abelev *et al.*, “Charged kaon femtoscopic correlations in pp collisions at $\sqrt{s} = 7$ TeV”, *Phys. Rev. D* **87** (2013) 052016, arXiv:1212.5958 [hep-ex].
- [64] ALICE Collaboration, K. Aamodt *et al.*, “Femtосcopy of pp collisions at $\sqrt{s} = 0.9$ and 7 TeV at the LHC with two-pion Bose-Einstein correlations”, *Phys. Rev. D* **84** (2011) 112004, arXiv:1101.3665 [hep-ex].
- [65] ALICE Collaboration, J. Adam *et al.*, “Two-pion femtосcopy in p-Pb collisions at $\sqrt{s_{NN}} = 5.02$ TeV”, *Phys. Rev. C* **91** (2015) 034906, arXiv:1502.00559 [nucl-ex].
- [66] ALICE Collaboration, S. Acharya *et al.*, “Multiplicity dependence of (multi-)strange hadron production in proton–proton collisions at $\sqrt{s} = 13$ TeV”, *Eur. Phys. J. C* **80** (2020) 167, arXiv:1908.01861 [nucl-ex].
- [67] R. Lednický and V. Lyuboshits, “Final State Interaction Effect on Pairing Correlations Between Particles with Small Relative Momenta”, *Sov. J. Nucl. Phys.* **35** (1982) 770.
- [68] S. M. Flatte, “Coupled - Channel Analysis of the $\pi\eta$ and K anti-K Systems Near K anti-K Threshold”, *Phys. Lett. B* **63** (1976) 224–227.
- [69] F. Giacosa, A. Okopińska, and V. Shashy, “A simple alternative to the relativistic Breit–Wigner distribution”, *Eur. Phys. J. A* **57** (2021) 336, arXiv:2106.03749 [hep-ph].
- [70] V. Baru, J. Haidenbauer, C. Hanhart, A. E. Kudryavtsev, and U.-G. Meissner, “Flatte-like distributions and the $a_0(980)/f_0(980)$ mesons”, *Eur. Phys. J. A* **23** (2005) 523–533, arXiv:nucl-th/0410099.
- [71] A. Feijoo, V. Valcarce, and V. K. Magas, “The $\Xi(1620)$ and $\Xi(1690)$ molecular states from $S = -2$ meson-baryon interaction up to next-to-leading order”, *Phys. Lett. B* **841** (4, 2023) 137927, arXiv:2303.01323 [hep-ph].

A The ALICE Collaboration

S. Acharya ¹²⁶, D. Adamová ⁸⁷, A. Adler⁷⁰, G. Aglieri Rinella ³³, M. Agnello ³⁰, N. Agrawal ⁵¹, Z. Ahammed ¹³³, S. Ahmad ¹⁶, S.U. Ahn ⁷¹, I. Ahuja ³⁸, A. Akindinov ¹⁴¹, M. Al-Turany ⁹⁸, D. Aleksandrov ¹⁴¹, B. Alessandro ⁵⁶, H.M. Alfanda ⁶, R. Alfaro Molina ⁶⁷, B. Ali ¹⁶, A. Alici ²⁶, N. Alizadehvandchali ¹¹⁵, A. Alkin ³³, J. Alme ²¹, G. Alocco ⁵², T. Alt ⁶⁴, A.R. Altamura ⁵⁰, I. Altsybeev ⁹⁶, M.N. Anaam ⁶, C. Andrei ⁴⁶, A. Andronic ¹³⁶, V. Anguelov ⁹⁵, F. Antinori ⁵⁴, P. Antonioli ⁵¹, N. Apadula ⁷⁵, L. Aphecetche ¹⁰⁴, H. Appelshäuser ⁶⁴, C. Arata ⁷⁴, S. Arcelli ²⁶, M. Aresti ⁵², R. Arnaldi ⁵⁶, J.G.M.C.A. Arneiro ¹¹¹, I.C. Arsene ²⁰, M. Arslanok ¹³⁸, A. Augustinus ³³, R. Averbeck ⁹⁸, M.D. Azmi ¹⁶, H. Baba¹²³, A. Badalà ⁵³, J. Bae ¹⁰⁵, Y.W. Baek ⁴¹, X. Bai ¹¹⁹, R. Bailhache ⁶⁴, Y. Bailung ⁴⁸, A. Balbino ³⁰, A. Baldisseri ¹²⁹, B. Balis ², D. Banerjee ⁴, Z. Banoo ⁹², R. Barbera ²⁷, F. Barile ³², L. Barioglio ⁹⁶, M. Barlou⁷⁹, G.G. Barnaföldi ¹³⁷, L.S. Barnby ⁸⁶, V. Barret ¹²⁶, L. Barreto ¹¹¹, C. Bartels ¹¹⁸, K. Barth ³³, E. Bartsch ⁶⁴, N. Bastid ¹²⁶, S. Basu ⁷⁶, G. Batigne ¹⁰⁴, D. Battistini ⁹⁶, B. Batyunya ¹⁴², D. Bauri⁴⁷, J.L. Bazo Alba ¹⁰², I.G. Bearden ⁸⁴, C. Beattie ¹³⁸, P. Becht ⁹⁸, D. Behera ⁴⁸, I. Belikov ¹²⁸, A.D.C. Bell Hechavarria ¹³⁶, F. Bellini ²⁶, R. Bellwied ¹¹⁵, S. Belokurova ¹⁴¹, G. Bencedi ¹³⁷, S. Beole ²⁵, A. Bercuci ⁴⁶, Y. Berdnikov ¹⁴¹, A. Berdnikova ⁹⁵, L. Bergmann ⁹⁵, M.G. Besoiu ⁶³, L. Betev ³³, P.P. Bhaduri ¹³³, A. Bhasin ⁹², M.A. Bhat ⁴, B. Bhattacharjee ⁴², L. Bianchi ²⁵, N. Bianchi ⁴⁹, J. Bielčik ³⁶, J. Bielčíková ⁸⁷, J. Biernat ¹⁰⁸, A.P. Bigot ¹²⁸, A. Bilandzic ⁹⁶, G. Biro ¹³⁷, S. Biswas ⁴, N. Bize ¹⁰⁴, J.T. Blair ¹⁰⁹, D. Blau ¹⁴¹, M.B. Blidaru ⁹⁸, N. Bluhme³⁹, C. Blume ⁶⁴, G. Boca ^{22,55}, F. Bock ⁸⁸, T. Bodova ²¹, A. Bogdanov¹⁴¹, S. Boi ²³, J. Bok ⁵⁸, L. Boldizsár ¹³⁷, M. Bombara ³⁸, P.M. Bond ³³, G. Bonomi ^{132,55}, H. Borel ¹²⁹, A. Borissov ¹⁴¹, A.G. Borquez Carcamo ⁹⁵, H. Bossi ¹³⁸, E. Botta ²⁵, Y.E.M. Bouziani ⁶⁴, L. Bratrud ⁶⁴, P. Braun-Munzinger ⁹⁸, M. Bregant ¹¹¹, M. Broz ³⁶, G.E. Bruno ^{97,32}, M.D. Buckland ²⁴, D. Budnikov ¹⁴¹, H. Buesching ⁶⁴, S. Bufalino ³⁰, P. Buhler ¹⁰³, N. Burmasov ¹⁴¹, Z. Buthelezi ^{68,122}, A. Bylinkin ²¹, S.A. Bysiak¹⁰⁸, M. Cai ⁶, H. Caines ¹³⁸, A. Caliva ²⁹, E. Calvo Villar ¹⁰², J.M.M. Camacho ¹¹⁰, P. Camerini ²⁴, F.D.M. Canedo ¹¹¹, M. Carabas ¹²⁵, A.A. Carballo ³³, F. Carnesecchi ³³, R. Caron ¹²⁷, L.A.D. Carvalho ¹¹¹, J. Castillo Castellanos ¹²⁹, F. Catalano ^{33,25}, C. Ceballos Sanchez ¹⁴², I. Chakaberia ⁷⁵, P. Chakraborty ⁴⁷, S. Chandra ¹³³, S. Chapeland ³³, M. Chartier ¹¹⁸, S. Chattopadhyay ¹³³, S. Chattopadhyay ¹⁰⁰, T.G. Chavez ⁴⁵, T. Cheng ^{98,6}, C. Cheshkov ¹²⁷, B. Cheynis ¹²⁷, V. Chibante Barroso ³³, D.D. Chinellato ¹¹², E.S. Chizzali ^{1,96}, J. Cho ⁵⁸, S. Cho ⁵⁸, P. Chochula ³³, P. Christakoglou ⁸⁵, C.H. Christensen ⁸⁴, P. Christiansen ⁷⁶, T. Chujo ¹²⁴, M. Ciacco ³⁰, C. Cicalo ⁵², F. Cindolo ⁵¹, M.R. Ciupek⁹⁸, G. Clai^{II,51}, F. Colamaria ⁵⁰, J.S. Colburn¹⁰¹, D. Colella ^{97,32}, M. Colocci ²⁶, G. Conesa Balbastre ⁷⁴, Z. Conesa del Valle ⁷³, G. Contin ²⁴, J.G. Contreras ³⁶, M.L. Coquet ¹²⁹, P. Cortese ^{131,56}, M.R. Cosentino ¹¹³, F. Costa ³³, S. Costanza ^{22,55}, C. Cot ⁷³, J. Crkovská ⁹⁵, P. Crochet ¹²⁶, R. Cruz-Torres ⁷⁵, P. Cui ⁶, A. Dainese ⁵⁴, M.C. Danisch ⁹⁵, A. Danu ⁶³, P. Das ⁸¹, P. Das ⁴, S. Das ⁴, A.R. Dash ¹³⁶, S. Dash ⁴⁷, R.M.H. David⁴⁵, A. De Caro ²⁹, G. de Cataldo ⁵⁰, J. de Cuveland³⁹, A. De Falco ²³, D. De Gruttola ²⁹, N. De Marco ⁵⁶, C. De Martin ²⁴, S. De Pasquale ²⁹, R. Deb ¹³², S. Deb ⁴⁸, R. Del Grande ⁹⁶, L. Dello Stritto ²⁹, W. Deng ⁶, P. Dhankher ¹⁹, D. Di Bari ³², A. Di Mauro ³³, B. Diab ¹²⁹, R.A. Diaz ^{142,7}, T. Dietel ¹¹⁴, Y. Ding ⁶, R. Divià ³³, D.U. Dixit ¹⁹, Ø. Djuvland²¹, U. Dmitrieva ¹⁴¹, A. Dobrin ⁶³, B. Dönigus ⁶⁴, J.M. Dubinski ¹³⁴, A. Dubla ⁹⁸, S. Dudi ⁹¹, P. Dupieux ¹²⁶, M. Durkac ¹⁰⁷, N. Dzalaiova¹³, T.M. Eder ¹³⁶, R.J. Ehlers ⁷⁵, F. Eisenhut ⁶⁴, R. Ejima⁹³, D. Elia ⁵⁰, B. Erazmus ¹⁰⁴, F. Ercolessi ²⁶, F. Erhardt ⁹⁰, M.R. Ersdal²¹, B. Espagnon ⁷³, G. Eulisse ³³, D. Evans ¹⁰¹, S. Evdokimov ¹⁴¹, L. Fabbietti ⁹⁶, M. Faggin ²⁸, J. Faivre ⁷⁴, F. Fan ⁶, W. Fan ⁷⁵, A. Fantoni ⁴⁹, M. Fasel ⁸⁸, P. Fedchio³⁰, A. Feliciello ⁵⁶, G. Feofilov ¹⁴¹, A. Fernández Téllez ⁴⁵, L. Ferrandi ¹¹¹, M.B. Ferrer ³³, A. Ferrero ¹²⁹, C. Ferrero ⁵⁶, A. Ferretti ²⁵, V.J.G. Feuillard ⁹⁵, V. Filova ³⁶, D. Finogeev ¹⁴¹, F.M. Fionda ⁵², F. Flor ¹¹⁵, A.N. Flores ¹⁰⁹, S. Foertsch ⁶⁸, I. Fokin ⁹⁵, S. Fokin ¹⁴¹, E. Fragiocomo ⁵⁷, E. Frajna ¹³⁷, U. Fuchs ³³, N. Funicello ²⁹, C. Furget ⁷⁴, A. Furs ¹⁴¹, T. Fusayasu ⁹⁹, J.J. Gaardhøje ⁸⁴, M. Gagliardi ²⁵, A.M. Gago ¹⁰², T. Gahlaut⁴⁷, C.D. Galvan ¹¹⁰, D.R. Gangadharan ¹¹⁵, P. Ganoti ⁷⁹, C. Garabatos ⁹⁸, A.T. Garcia ⁷³, J.R.A. Garcia ⁴⁵, E. Garcia-Solis ⁹, C. Gargiulo ³³, K. Garner¹³⁶, P. Gasik ⁹⁸, A. Gautam ¹¹⁷, M.B. Gay Ducati ⁶⁶, M. Germain ¹⁰⁴, A. Ghimouz¹²⁴, C. Ghosh¹³³, M. Giacalone ⁵¹, G. Gioachin ³⁰, P. Giubellino ^{98,56}, P. Giubilato ²⁸, A.M.C. Glaenger ¹²⁹, P. Glässel ⁹⁵, E. Glimos ¹²¹, D.J.Q. Goh⁷⁷, V. Gonzalez ¹³⁵, M. Gorgon ², K. Goswami ⁴⁸, S. Gotovac³⁴, V. Grabski ⁶⁷, L.K. Graczykowski ¹³⁴, E. Grecka ⁸⁷, A. Grelli ⁵⁹, C. Grigoras ³³, V. Grigoriev ¹⁴¹, S. Grigoryan ^{142,1}, F. Grosa ³³, J.F. Grosse-Oetringhaus ³³, R. Grosso ⁹⁸, D. Grund ³⁶, G.G. Guardianio ¹¹², R. Guernane ⁷⁴, M. Guilbaud ¹⁰⁴, K. Gulbrandsen ⁸⁴, T. Gundem ⁶⁴, T. Gunji ¹²³, W. Guo ⁶, A. Gupta ⁹², R. Gupta ⁹²,

R. Gupta ⁴⁸, S.P. Guzman ⁴⁵, K. Gwizdzziel ¹³⁴, L. Gyulai ¹³⁷, C. Hadjidakis ⁷³, F.U. Haider ⁹², H. Hamagaki ⁷⁷, A. Hamdi ⁷⁵, Y. Han ¹³⁹, B.G. Hanley ¹³⁵, R. Hannigan ¹⁰⁹, J. Hansen ⁷⁶, M.R. Haque ¹³⁴, J.W. Harris ¹³⁸, A. Harton ⁹, H. Hassan ⁸⁸, D. Hatzifotiadou ⁵¹, P. Hauer ⁴³, L.B. Havener ¹³⁸, S.T. Heckel ⁹⁶, E. Hellbär ⁹⁸, H. Helstrup ³⁵, M. Hemmer ⁶⁴, T. Herman ³⁶, G. Herrera Corral ⁸, F. Herrmann ¹³⁶, S. Herrmann ¹²⁷, K.F. Hetland ³⁵, B. Heybeck ⁶⁴, H. Hillemanns ³³, B. Hippolyte ¹²⁸, F.W. Hoffmann ⁷⁰, B. Hofman ⁵⁹, G.H. Hong ¹³⁹, M. Horst ⁹⁶, A. Horzyk ², Y. Hou ⁶, P. Hristov ³³, C. Hughes ¹²¹, P. Huhn ⁶⁴, L.M. Huhta ¹¹⁶, T.J. Humanic ⁸⁹, A. Hutson ¹¹⁵, D. Hutter ³⁹, R. Ilkaev ¹⁴¹, H. Ilyas ¹⁴, M. Inaba ¹²⁴, G.M. Innocenti ³³, M. Ippolitov ¹⁴¹, A. Isakov ^{85,87}, T. Isidori ¹¹⁷, M.S. Islam ¹⁰⁰, M. Ivanov ¹³, M. Ivanov ⁹⁸, V. Ivanov ¹⁴¹, K.E. Iversen ⁷⁶, M. Jablonski ², B. Jacak ⁷⁵, N. Jacazio ²⁶, P.M. Jacobs ⁷⁵, S. Jadlovská ¹⁰⁷, J. Jadlovsky ¹⁰⁷, S. Jaelani ⁸³, C. Jahnke ¹¹², M.J. Jakubowska ¹³⁴, M.A. Janik ¹³⁴, T. Janson ⁷⁰, S. Ji ¹⁷, S. Jia ¹⁰, A.A.P. Jimenez ⁶⁵, F. Jonas ⁸⁸, D.M. Jones ¹¹⁸, J.M. Jowett ^{33,98}, J. Jung ⁶⁴, M. Jung ⁶⁴, A. Junique ³³, A. Jusko ¹⁰¹, M.J. Kabus ^{33,134}, J. Kaewjai ¹⁰⁶, P. Kalinak ⁶⁰, A.S. Kalteyer ⁹⁸, A. Kalweit ³³, V. Kaplin ¹⁴¹, A. Karasu Uysal ⁷², D. Karatovic ⁹⁰, O. Karavichev ¹⁴¹, T. Karavicheva ¹⁴¹, P. Karczmarczyk ¹³⁴, E. Karpechev ¹⁴¹, U. Kebschull ⁷⁰, R. Keidel ¹⁴⁰, D.L.D. Keijdener ⁵⁹, M. Keil ³³, B. Ketzer ⁴³, S.S. Khade ⁴⁸, A.M. Khan ^{119,6}, S. Khan ¹⁶, A. Khanzadeev ¹⁴¹, Y. Kharlov ¹⁴¹, A. Khatun ¹¹⁷, A. Khuntia ³⁶, M.B. Kidson ¹¹⁴, B. Kileng ³⁵, B. Kim ¹⁰⁵, C. Kim ¹⁷, D.J. Kim ¹¹⁶, E.J. Kim ⁶⁹, J. Kim ¹³⁹, J.S. Kim ⁴¹, J. Kim ⁵⁸, J. Kim ⁶⁹, M. Kim ¹⁹, S. Kim ¹⁸, T. Kim ¹³⁹, K. Kimura ⁹³, S. Kirsch ⁶⁴, I. Kisel ³⁹, S. Kiselev ¹⁴¹, A. Kisiel ¹³⁴, J.P. Kitowski ², J.L. Klay ⁵, J. Klein ³³, S. Klein ⁷⁵, C. Klein-Bösing ¹³⁶, M. Kleiner ⁶⁴, T. Klemenz ⁹⁶, A. Kluge ³³, A.G. Knospe ¹¹⁵, C. Kobdaj ¹⁰⁶, T. Kollegger ⁹⁸, A. Kondratyev ¹⁴², N. Kondratyeva ¹⁴¹, E. Kondratyuk ¹⁴¹, J. König ⁶⁴, S.A. Königstorfer ⁹⁶, P.J. Konopka ³³, G. Kornakov ¹³⁴, S.D. Koryciak ², A. Kotliarov ⁸⁷, V. Kovalenko ¹⁴¹, M. Kowalski ¹⁰⁸, V. Kozuharov ³⁷, I. Králik ⁶⁰, A. Kravčáková ³⁸, L. Krcal ^{33,39}, M. Krivda ^{101,60}, F. Krizek ⁸⁷, K. Krizkova Gajdosova ³³, M. Kroesen ⁹⁵, M. Krüger ⁶⁴, D.M. Krupova ³⁶, E. Kryshen ¹⁴¹, V. Kučera ⁵⁸, C. Kuhn ¹²⁸, P.G. Kuijter ⁸⁵, T. Kumaoka ¹²⁴, D. Kumar ¹³³, L. Kumar ⁹¹, N. Kumar ⁹¹, S. Kumar ³², S. Kundu ³³, P. Kurashvili ⁸⁰, A. Kurepin ¹⁴¹, A.B. Kurepin ¹⁴¹, A. Kuryakin ¹⁴¹, S. Kushpil ⁸⁷, M.J. Kweon ⁵⁸, Y. Kwon ¹³⁹, S.L. La Pointe ³⁹, P. La Rocca ²⁷, A. Lakrathok ¹⁰⁶, M. Lamanna ³³, R. Langoy ¹²⁰, P. Larionov ³³, E. Laudi ³³, L. Lautner ^{33,96}, R. Lavicka ¹⁰³, R. Lea ^{132,55}, H. Lee ¹⁰⁵, I. Legrand ⁴⁶, G. Legras ¹³⁶, J. Lehrbach ³⁹, T.M. Lelek ², R.C. Lemmon ⁸⁶, I. León Monzón ¹¹⁰, M.M. Lesch ⁹⁶, E.D. Lesser ¹⁹, P. Lévai ¹³⁷, X. Li ¹⁰, X.L. Li ⁶, J. Lien ¹²⁰, R. Lietava ¹⁰¹, I. Likmeta ¹¹⁵, B. Lim ²⁵, S.H. Lim ¹⁷, V. Lindenstruth ³⁹, A. Lindner ⁴⁶, C. Lippmann ⁹⁸, A. Liu ¹⁹, D.H. Liu ⁶, J. Liu ¹¹⁸, G.S.S. Liveraro ¹¹², I.M. Lofnes ²¹, C. Loizides ⁸⁸, S. Lokos ¹⁰⁸, J. Lomker ⁵⁹, P. Loncar ³⁴, X. Lopez ¹²⁶, E. López Torres ⁷, P. Lu ^{98,119}, J.R. Luhder ¹³⁶, M. Lunardon ²⁸, G. Luparello ⁵⁷, Y.G. Ma ⁴⁰, M. Mager ³³, A. Maire ¹²⁸, M.V. Makariev ³⁷, M. Malaev ¹⁴¹, G. Malfattore ²⁶, N.M. Malik ⁹², Q.W. Malik ²⁰, S.K. Malik ⁹², L. Malinina ¹⁴², D. Mallick ^{73,81}, N. Mallick ⁴⁸, G. Mandaglio ^{31,53}, S.K. Mandal ⁸⁰, V. Manko ¹⁴¹, F. Manso ¹²⁶, V. Manzari ⁵⁰, Y. Mao ⁶, R.W. Marcjan ², G.V. Margagliotti ²⁴, A. Margotti ⁵¹, A. Marín ⁹⁸, C. Markert ¹⁰⁹, P. Martinengo ³³, M.I. Martínez ⁴⁵, G. Martínez García ¹⁰⁴, M.P.P. Martins ¹¹¹, S. Masciocchi ⁹⁸, M. Masera ²⁵, A. Masoni ⁵², L. Massacrier ⁷³, O. Massen ⁵⁹, A. Mastroserio ^{130,50}, O. Matonoha ⁷⁶, S. Mattiazzo ²⁸, P.F.T. Matuoka ¹¹¹, A. Matyja ¹⁰⁸, C. Mayer ¹⁰⁸, A.L. Mazuecos ³³, F. Mazzaschi ²⁵, M. Mazzilli ³³, J.E. Mdhuli ¹²², A.F. Mechler ⁶⁴, Y. Melikyan ⁴⁴, A. Menchaca-Rocha ⁶⁷, E. Meninno ^{103,29}, A.S. Menon ¹¹⁵, M. Meres ¹³, S. Mhlanga ^{114,68}, Y. Miake ¹²⁴, L. Micheletti ³³, L.C. Migliorin ¹²⁷, D.L. Mihaylov ⁹⁶, K. Mikhaylov ^{142,141}, A.N. Mishra ¹³⁷, D. Miśkowiec ⁹⁸, A. Modak ⁴, A.P. Mohanty ⁵⁹, B. Mohanty ⁸¹, M. Mohisin Khan ^{III,16}, M.A. Molander ⁴⁴, S. Monira ¹³⁴, Z. Moravcova ⁸⁴, C. Mordasini ¹¹⁶, D.A. Moreira De Godoy ¹³⁶, I. Morozov ¹⁴¹, A. Morsch ³³, T. Mrnjavac ³³, V. Muccifora ⁴⁹, S. Muhuri ¹³³, J.D. Mulligan ⁷⁵, A. Mulliri ²³, M.G. Munhoz ¹¹¹, R.H. Munzer ⁶⁴, H. Murakami ¹²³, S. Murray ¹¹⁴, L. Musa ³³, J. Musinsky ⁶⁰, J.W. Myrcha ¹³⁴, B. Naik ¹²², A.I. Nambrath ¹⁹, B.K. Nandi ⁴⁷, R. Nania ⁵¹, E. Nappi ⁵⁰, A.F. Nassirpour ^{18,76}, A. Nath ⁹⁵, C. Nattrass ¹²¹, M.N. Naydenov ³⁷, A. Neagu ²⁰, A. Negru ¹²⁵, L. Nellen ⁶⁵, R. Nepeivoda ⁷⁶, S. Nese ²⁰, G. Neskovic ³⁹, B.S. Nielsen ⁸⁴, E.G. Nielsen ⁸⁴, S. Nikolaev ¹⁴¹, S. Nikulin ¹⁴¹, V. Nikulin ¹⁴¹, F. Noferini ⁵¹, S. Noh ¹², P. Nomokonov ¹⁴², J. Norman ¹¹⁸, N. Novitzky ¹²⁴, P. Nowakowski ¹³⁴, A. Nyanin ¹⁴¹, J. Nystrand ²¹, M. Ogino ⁷⁷, S. Oh ¹⁸, A. Ohlson ⁷⁶, V.A. Okorokov ¹⁴¹, J. Oleniacz ¹³⁴, A.C. Oliveira Da Silva ¹²¹, M.H. Oliver ¹³⁸, A. Onnerstad ¹¹⁶, C. Oppedisano ⁵⁶, A. Ortiz Velasquez ⁶⁵, J. Otwinowski ¹⁰⁸, M. Oya ⁹³, K. Oyama ⁷⁷, Y. Pachmayer ⁹⁵, S. Padhan ⁴⁷, D. Pagano ^{132,55}, G. Paic ⁶⁵, A. Palasciano ⁵⁰,

S. Panebianco ¹²⁹, H. Park ¹²⁴, H. Park ¹⁰⁵, J. Park ⁵⁸, J.E. Parkkila ³³, Y. Patley ⁴⁷, R.N. Patra ⁹²,
 B. Paul ²³, H. Pei ⁶, T. Peitzmann ⁵⁹, X. Peng ¹¹, M. Pennisi ²⁵, S. Perciballi ²⁵, D. Peresunko ¹⁴¹,
 G.M. Perez ⁷, Y. Pestov ¹⁴¹, V. Petrov ¹⁴¹, M. Petrovici ⁴⁶, R.P. Pezzi ^{104,66}, S. Piano ⁵⁷, M. Pikna ¹³,
 P. Pillot ¹⁰⁴, O. Pinazza ^{51,33}, L. Pinsky ¹¹⁵, C. Pinto ⁹⁶, S. Pisano ⁴⁹, M. Płoskoń ⁷⁵, M. Planinic ⁹⁰,
 F. Pliquett ⁶⁴, M.G. Poghosyan ⁸⁸, B. Polichtchouk ¹⁴¹, S. Politano ³⁰, N. Poljak ⁹⁰, A. Pop ⁴⁶,
 S. Porteboeuf-Houssais ¹²⁶, V. Pozdniakov ¹⁴², I.Y. Pozos ⁴⁵, K.K. Pradhan ⁴⁸, S.K. Prasad ⁴,
 S. Prasad ⁴⁸, R. Preghenella ⁵¹, F. Prino ⁵⁶, C.A. Pruneau ¹³⁵, I. Pshenichnov ¹⁴¹, M. Puccio ³³,
 S. Pucillo ²⁵, Z. Pugelova ¹⁰⁷, S. Qiu ⁸⁵, L. Quaglia ²⁵, R.E. Quishpe ¹¹⁵, S. Ragoni ¹⁵,
 A. Rakotozafindrabe ¹²⁹, L. Ramello ^{131,56}, F. Rami ¹²⁸, S.A.R. Ramirez ⁴⁵, T.A. Rancien ⁷⁴, M. Rasa ²⁷,
 S.S. Räsänen ⁴⁴, R. Rath ⁵¹, M.P. Rauch ²¹, I. Ravasenga ⁸⁵, K.F. Read ^{88,121}, C. Reckziegel ¹¹³,
 A.R. Redelbach ³⁹, K. Redlich ^{IV,80}, C.A. Reetz ⁹⁸, A. Rehman ²¹, F. Reidt ³³, H.A. Reme-Ness ³⁵,
 Z. Rescakova ³⁸, K. Reygers ⁹⁵, A. Riabov ¹⁴¹, V. Riabov ¹⁴¹, R. Ricci ²⁹, M. Richter ²⁰,
 A.A. Riedel ⁹⁶, W. Riegler ³³, A.G. Riffero ²⁵, C. Ristea ⁶³, M.V. Rodriguez ³³, M. Rodríguez
 Cahuantzi ⁴⁵, K. Røed ²⁰, R. Rogalev ¹⁴¹, E. Rogochaya ¹⁴², T.S. Rogoschinski ⁶⁴, D. Rohr ³³,
 D. Röhrich ²¹, P.F. Rojas ⁴⁵, S. Rojas Torres ³⁶, P.S. Rokita ¹³⁴, G. Romanenko ²⁶, F. Ronchetti ⁴⁹,
 A. Rosano ^{31,53}, E.D. Rosas ⁶⁵, K. Roslon ¹³⁴, A. Rossi ⁵⁴, A. Roy ⁴⁸, S. Roy ⁴⁷, N. Rubini ²⁶,
 O.V. Rueda ¹¹⁵, D. Ruggiano ¹³⁴, R. Rui ²⁴, P.G. Russek ², R. Russo ⁸⁵, A. Rustamov ⁸²,
 E. Ryabinkin ¹⁴¹, Y. Ryabov ¹⁴¹, A. Rybicki ¹⁰⁸, H. Rytkonen ¹¹⁶, J. Ryu ¹⁷, W. Rzesza ¹³⁴,
 O.A.M. Saari ⁴⁴, S. Sadhu ³², S. Sadovsky ¹⁴¹, J. Saetre ²¹, K. Šafařík ³⁶, P. Saha ⁴², S.K. Saha ⁴,
 S. Saha ⁸¹, B. Sahoo ⁴⁷, B. Sahoo ⁴⁸, R. Sahoo ⁴⁸, S. Sahoo ⁶¹, D. Sahu ⁴⁸, P.K. Sahu ⁶¹, J. Saini ¹³³,
 K. Sajdakova ³⁸, S. Sakai ¹²⁴, M.P. Salvan ⁹⁸, S. Sambyal ⁹², D. Samitz ¹⁰³, I. Sanna ^{33,96},
 T.B. Saramela ¹¹¹, D. Sarkar ¹³⁵, P. Sarma ⁴², V. Sarritzu ²³, V.M. Sarti ⁹⁶, M.H.P. Sas ¹³⁸,
 J. Schambach ⁸⁸, H.S. Scheid ⁶⁴, C. Schiaua ⁴⁶, R. Schicker ⁹⁵, A. Schmah ⁹⁸, C. Schmidt ⁹⁸,
 H.R. Schmidt ⁹⁴, M.O. Schmidt ³³, M. Schmidt ⁹⁴, N.V. Schmidt ⁸⁸, A.R. Schmier ¹²¹, R. Schotter ¹²⁸,
 A. Schröter ³⁹, J. Schukraft ³³, K. Schweda ⁹⁸, G. Scioli ²⁶, E. Scomparin ⁵⁶, J.E. Seger ¹⁵,
 Y. Sekiguchi ¹²³, D. Sekihata ¹²³, M. Selina ⁸⁵, I. Selyuzhenkov ⁹⁸, S. Senyukov ¹²⁸, J.J. Seo ^{95,58},
 D. Serebryakov ¹⁴¹, L. Šerkšnytė ⁹⁶, A. Sevcenco ⁶³, T.J. Shaba ⁶⁸, A. Shabetai ¹⁰⁴, R. Shahoyan ³³,
 A. Shangaraev ¹⁴¹, A. Sharma ⁹¹, B. Sharma ⁹², D. Sharma ⁴⁷, H. Sharma ^{54,108}, M. Sharma ⁹²,
 S. Sharma ⁷⁷, S. Sharma ⁹², U. Sharma ⁹², A. Shatat ⁷³, O. Sheibani ¹¹⁵, K. Shigaki ⁹³, M. Shimomura ⁷⁸,
 J. Shin ¹², S. Shirinkin ¹⁴¹, Q. Shou ⁴⁰, Y. Sibiriak ¹⁴¹, S. Siddhanta ⁵², T. Siemiarczuk ⁸⁰,
 T.F. Silva ¹¹¹, D. Silvermyr ⁷⁶, T. Simantathammakul ¹⁰⁶, R. Simeonov ³⁷, B. Singh ⁹², B. Singh ⁹⁶,
 K. Singh ⁴⁸, R. Singh ⁸¹, R. Singh ⁹², R. Singh ⁴⁸, S. Singh ¹⁶, V.K. Singh ¹³³, V. Singhal ¹³³,
 T. Sinha ¹⁰⁰, B. Sitar ¹³, M. Sitta ^{131,56}, T.B. Skaali ²⁰, G. Skorodumovs ⁹⁵, M. Slupecki ⁴⁴,
 N. Smirnov ¹³⁸, R.J.M. Snellings ⁵⁹, E.H. Solheim ²⁰, J. Song ¹¹⁵, A. Songmoolnak ¹⁰⁶,
 C. Sonnabend ^{33,98}, F. Soramel ²⁸, A.B. Soto-hernandez ⁸⁹, R. Spijkers ⁸⁵, I. Sputowska ¹⁰⁸, J. Staa ⁷⁶,
 J. Stachel ⁹⁵, I. Stan ⁶³, P.J. Steffanic ¹²¹, S.F. Stiefelmaier ⁹⁵, D. Stocco ¹⁰⁴, I. Storehaug ²⁰,
 P. Stratmann ¹³⁶, S. Strazzi ²⁶, A. Sturmiolo ^{31,53}, C.P. Stylianidis ⁸⁵, A.A.P. Suaide ¹¹¹, C. Suire ⁷³,
 M. Sukhanov ¹⁴¹, M. Suljic ³³, R. Sultanov ¹⁴¹, V. Sumberia ⁹², S. Sumowidagdo ⁸³, S. Swain ⁶¹,
 I. Szarka ¹³, M. Szymkowski ¹³⁴, S.F. Taghavi ⁹⁶, G. Taillepied ⁹⁸, J. Takahashi ¹¹², G.J. Tambave ⁸¹,
 S. Tang ⁶, Z. Tang ¹¹⁹, J.D. Tapia Takaki ¹¹⁷, N. Tapus ¹²⁵, L.A. Tarasovicova ¹³⁶, M.G. Tarzila ⁴⁶,
 G.F. Tassielli ³², A. Tauro ³³, G. Tejeda Muñoz ⁴⁵, A. Telesca ³³, L. Terlizzi ²⁵, C. Terrevoli ¹¹⁵,
 S. Thakur ⁴, D. Thomas ¹⁰⁹, A. Tikhonov ¹⁴¹, A.R. Timmins ¹¹⁵, M. Tkacik ¹⁰⁷, T. Tkacik ¹⁰⁷,
 A. Toia ⁶⁴, R. Tokumoto ⁹³, K. Tomohiro ⁹³, N. Topilskaya ¹⁴¹, M. Toppi ⁴⁹, T. Tork ⁷³, V.V. Torres ¹⁰⁴,
 A.G. Torres Ramos ³², A. Trifiró ^{31,53}, A.S. Triolo ^{33,31,53}, S. Tripathy ⁵¹, T. Tripathy ⁴⁷, S. Trogolo ³³,
 V. Trubnikov ³, W.H. Trzaska ¹¹⁶, T.P. Trzcinski ¹³⁴, A. Tumkin ¹⁴¹, R. Turrisi ⁵⁴, T.S. Tveter ²⁰,
 K. Ullaland ²¹, B. Ulukutlu ⁹⁶, A. Uras ¹²⁷, G.L. Usai ²³, M. Vala ³⁸, N. Valle ²², L.V.R. van
 Doremalen ⁵⁹, M. van Leeuwen ⁸⁵, C.A. van Veen ⁹⁵, R.J.G. van Weelden ⁸⁵, P. Vande Vyvre ³³,
 D. Varga ¹³⁷, Z. Varga ¹³⁷, M. Vasileiou ⁷⁹, A. Vasiliev ¹⁴¹, O. Vázquez Doce ⁴⁹, V. Vechernin ¹⁴¹,
 E. Vercellin ²⁵, S. Vergara Limón ⁴⁵, R. Verma ⁴⁷, L. Vermunt ⁹⁸, R. Vértesi ¹³⁷, M. Verweij ⁵⁹,
 L. Vickovic ³⁴, Z. Vilakazi ¹²², O. Villalobos Baillie ¹⁰¹, A. Villani ²⁴, G. Vino ⁵⁰, A. Vinogradov ¹⁴¹,
 T. Virgili ²⁹, M.M.O. Virta ¹¹⁶, V. Vislavicius ⁷⁶, A. Vodopyanov ¹⁴², B. Volkel ³³, M.A. Völkl ⁹⁵,
 K. Voloshin ¹⁴¹, S.A. Voloshin ¹³⁵, G. Volpe ³², B. von Haller ³³, I. Vorobyev ⁹⁶, N. Vozniuk ¹⁴¹,
 J. Vrláková ³⁸, J. Wan ⁴⁰, C. Wang ⁴⁰, D. Wang ⁴⁰, Y. Wang ⁴⁰, Y. Wang ⁶, A. Wegrzynek ³³,
 F.T. Weiglhofer ³⁹, S.C. Wenzel ³³, J.P. Wessels ¹³⁶, S.L. Weyhmler ¹³⁸, J. Wiechula ⁶⁴, J. Wikne ²⁰,
 G. Wilk ⁸⁰, J. Wilkinson ⁹⁸, G.A. Willems ¹³⁶, B. Windelband ⁹⁵, M. Winn ¹²⁹, J.R. Wright ¹⁰⁹,
 W. Wu ⁴⁰, Y. Wu ¹¹⁹, R. Xu ⁶, A. Yadav ⁴³, A.K. Yadav ¹³³, S. Yalcin ⁷², Y. Yamaguchi ⁹³, S. Yang ²¹,

S. Yano ⁹³, Z. Yin ⁶, I.-K. Yoo ¹⁷, J.H. Yoon ⁵⁸, H. Yu¹², S. Yuan²¹, A. Yuncu ⁹⁵, V. Zaccolo ²⁴, C. Zampolli ³³, F. Zanone ⁹⁵, N. Zardoshti ³³, A. Zarochentsev ¹⁴¹, P. Závada ⁶², N. Zaviyalov¹⁴¹, M. Zhalov ¹⁴¹, B. Zhang ⁶, C. Zhang ¹²⁹, L. Zhang ⁴⁰, S. Zhang ⁴⁰, X. Zhang ⁶, Y. Zhang¹¹⁹, Z. Zhang ⁶, M. Zhao ¹⁰, V. Zherebchevskii ¹⁴¹, Y. Zhi¹⁰, D. Zhou ⁶, Y. Zhou ⁸⁴, J. Zhu ^{98,6}, Y. Zhu⁶, S.C. Zugravel ⁵⁶, N. Zurlo ^{132,55}

Affiliation Notes

^I Also at: Max-Planck-Institut für Physik, Munich, Germany

^{II} Also at: Italian National Agency for New Technologies, Energy and Sustainable Economic Development (ENEA), Bologna, Italy

^{III} Also at: Department of Applied Physics, Aligarh Muslim University, Aligarh, India

^{IV} Also at: Institute of Theoretical Physics, University of Wrocław, Poland

^V Also at: An institution covered by a cooperation agreement with CERN

Collaboration Institutes

¹ A.I. Alikhanyan National Science Laboratory (Yerevan Physics Institute) Foundation, Yerevan, Armenia

² AGH University of Science and Technology, Cracow, Poland

³ Bogolyubov Institute for Theoretical Physics, National Academy of Sciences of Ukraine, Kiev, Ukraine

⁴ Bose Institute, Department of Physics and Centre for Astroparticle Physics and Space Science (CAPSS), Kolkata, India

⁵ California Polytechnic State University, San Luis Obispo, California, United States

⁶ Central China Normal University, Wuhan, China

⁷ Centro de Aplicaciones Tecnológicas y Desarrollo Nuclear (CEADEN), Havana, Cuba

⁸ Centro de Investigación y de Estudios Avanzados (CINVESTAV), Mexico City and Mérida, Mexico

⁹ Chicago State University, Chicago, Illinois, United States

¹⁰ China Institute of Atomic Energy, Beijing, China

¹¹ China University of Geosciences, Wuhan, China

¹² Chungbuk National University, Cheongju, Republic of Korea

¹³ Comenius University Bratislava, Faculty of Mathematics, Physics and Informatics, Bratislava, Slovak Republic

¹⁴ COMSATS University Islamabad, Islamabad, Pakistan

¹⁵ Creighton University, Omaha, Nebraska, United States

¹⁶ Department of Physics, Aligarh Muslim University, Aligarh, India

¹⁷ Department of Physics, Pusan National University, Pusan, Republic of Korea

¹⁸ Department of Physics, Sejong University, Seoul, Republic of Korea

¹⁹ Department of Physics, University of California, Berkeley, California, United States

²⁰ Department of Physics, University of Oslo, Oslo, Norway

²¹ Department of Physics and Technology, University of Bergen, Bergen, Norway

²² Dipartimento di Fisica, Università di Pavia, Pavia, Italy

²³ Dipartimento di Fisica dell'Università and Sezione INFN, Cagliari, Italy

²⁴ Dipartimento di Fisica dell'Università and Sezione INFN, Trieste, Italy

²⁵ Dipartimento di Fisica dell'Università and Sezione INFN, Turin, Italy

²⁶ Dipartimento di Fisica e Astronomia dell'Università and Sezione INFN, Bologna, Italy

²⁷ Dipartimento di Fisica e Astronomia dell'Università and Sezione INFN, Catania, Italy

²⁸ Dipartimento di Fisica e Astronomia dell'Università and Sezione INFN, Padova, Italy

²⁹ Dipartimento di Fisica 'E.R. Caianiello' dell'Università and Gruppo Collegato INFN, Salerno, Italy

³⁰ Dipartimento DISAT del Politecnico and Sezione INFN, Turin, Italy

³¹ Dipartimento di Scienze MIFT, Università di Messina, Messina, Italy

³² Dipartimento Interateneo di Fisica 'M. Merlin' and Sezione INFN, Bari, Italy

³³ European Organization for Nuclear Research (CERN), Geneva, Switzerland

³⁴ Faculty of Electrical Engineering, Mechanical Engineering and Naval Architecture, University of Split, Split, Croatia

³⁵ Faculty of Engineering and Science, Western Norway University of Applied Sciences, Bergen, Norway

³⁶ Faculty of Nuclear Sciences and Physical Engineering, Czech Technical University in Prague, Prague, Czech Republic

- ³⁷ Faculty of Physics, Sofia University, Sofia, Bulgaria
³⁸ Faculty of Science, P.J. Šafárik University, Košice, Slovak Republic
³⁹ Frankfurt Institute for Advanced Studies, Johann Wolfgang Goethe-Universität Frankfurt, Frankfurt, Germany
⁴⁰ Fudan University, Shanghai, China
⁴¹ Gangneung-Wonju National University, Gangneung, Republic of Korea
⁴² Gauhati University, Department of Physics, Guwahati, India
⁴³ Helmholtz-Institut für Strahlen- und Kernphysik, Rheinische Friedrich-Wilhelms-Universität Bonn, Bonn, Germany
⁴⁴ Helsinki Institute of Physics (HIP), Helsinki, Finland
⁴⁵ High Energy Physics Group, Universidad Autónoma de Puebla, Puebla, Mexico
⁴⁶ Horia Hulubei National Institute of Physics and Nuclear Engineering, Bucharest, Romania
⁴⁷ Indian Institute of Technology Bombay (IIT), Mumbai, India
⁴⁸ Indian Institute of Technology Indore, Indore, India
⁴⁹ INFN, Laboratori Nazionali di Frascati, Frascati, Italy
⁵⁰ INFN, Sezione di Bari, Bari, Italy
⁵¹ INFN, Sezione di Bologna, Bologna, Italy
⁵² INFN, Sezione di Cagliari, Cagliari, Italy
⁵³ INFN, Sezione di Catania, Catania, Italy
⁵⁴ INFN, Sezione di Padova, Padova, Italy
⁵⁵ INFN, Sezione di Pavia, Pavia, Italy
⁵⁶ INFN, Sezione di Torino, Turin, Italy
⁵⁷ INFN, Sezione di Trieste, Trieste, Italy
⁵⁸ Inha University, Incheon, Republic of Korea
⁵⁹ Institute for Gravitational and Subatomic Physics (GRASP), Utrecht University/Nikhef, Utrecht, Netherlands
⁶⁰ Institute of Experimental Physics, Slovak Academy of Sciences, Košice, Slovak Republic
⁶¹ Institute of Physics, Homi Bhabha National Institute, Bhubaneswar, India
⁶² Institute of Physics of the Czech Academy of Sciences, Prague, Czech Republic
⁶³ Institute of Space Science (ISS), Bucharest, Romania
⁶⁴ Institut für Kernphysik, Johann Wolfgang Goethe-Universität Frankfurt, Frankfurt, Germany
⁶⁵ Instituto de Ciencias Nucleares, Universidad Nacional Autónoma de México, Mexico City, Mexico
⁶⁶ Instituto de Física, Universidade Federal do Rio Grande do Sul (UFRGS), Porto Alegre, Brazil
⁶⁷ Instituto de Física, Universidad Nacional Autónoma de México, Mexico City, Mexico
⁶⁸ iThemba LABS, National Research Foundation, Somerset West, South Africa
⁶⁹ Jeonbuk National University, Jeonju, Republic of Korea
⁷⁰ Johann-Wolfgang-Goethe Universität Frankfurt Institut für Informatik, Fachbereich Informatik und Mathematik, Frankfurt, Germany
⁷¹ Korea Institute of Science and Technology Information, Daejeon, Republic of Korea
⁷² KTO Karatay University, Konya, Turkey
⁷³ Laboratoire de Physique des 2 Infinis, Irène Joliot-Curie, Orsay, France
⁷⁴ Laboratoire de Physique Subatomique et de Cosmologie, Université Grenoble-Alpes, CNRS-IN2P3, Grenoble, France
⁷⁵ Lawrence Berkeley National Laboratory, Berkeley, California, United States
⁷⁶ Lund University Department of Physics, Division of Particle Physics, Lund, Sweden
⁷⁷ Nagasaki Institute of Applied Science, Nagasaki, Japan
⁷⁸ Nara Women's University (NWU), Nara, Japan
⁷⁹ National and Kapodistrian University of Athens, School of Science, Department of Physics, Athens, Greece
⁸⁰ National Centre for Nuclear Research, Warsaw, Poland
⁸¹ National Institute of Science Education and Research, Homi Bhabha National Institute, Jatni, India
⁸² National Nuclear Research Center, Baku, Azerbaijan
⁸³ National Research and Innovation Agency - BRIN, Jakarta, Indonesia
⁸⁴ Niels Bohr Institute, University of Copenhagen, Copenhagen, Denmark
⁸⁵ Nikhef, National institute for subatomic physics, Amsterdam, Netherlands
⁸⁶ Nuclear Physics Group, STFC Daresbury Laboratory, Daresbury, United Kingdom
⁸⁷ Nuclear Physics Institute of the Czech Academy of Sciences, Husinec-Řež, Czech Republic
⁸⁸ Oak Ridge National Laboratory, Oak Ridge, Tennessee, United States
⁸⁹ Ohio State University, Columbus, Ohio, United States

- ⁹⁰ Physics department, Faculty of science, University of Zagreb, Zagreb, Croatia
⁹¹ Physics Department, Panjab University, Chandigarh, India
⁹² Physics Department, University of Jammu, Jammu, India
⁹³ Physics Program and International Institute for Sustainability with Knotted Chiral Meta Matter (SKCM2), Hiroshima University, Hiroshima, Japan
⁹⁴ Physikalisches Institut, Eberhard-Karls-Universität Tübingen, Tübingen, Germany
⁹⁵ Physikalisches Institut, Ruprecht-Karls-Universität Heidelberg, Heidelberg, Germany
⁹⁶ Physik Department, Technische Universität München, Munich, Germany
⁹⁷ Politecnico di Bari and Sezione INFN, Bari, Italy
⁹⁸ Research Division and ExtreMe Matter Institute EMMI, GSI Helmholtzzentrum für Schwerionenforschung GmbH, Darmstadt, Germany
⁹⁹ Saga University, Saga, Japan
¹⁰⁰ Saha Institute of Nuclear Physics, Homi Bhabha National Institute, Kolkata, India
¹⁰¹ School of Physics and Astronomy, University of Birmingham, Birmingham, United Kingdom
¹⁰² Sección Física, Departamento de Ciencias, Pontificia Universidad Católica del Perú, Lima, Peru
¹⁰³ Stefan Meyer Institut für Subatomare Physik (SMI), Vienna, Austria
¹⁰⁴ SUBATECH, IMT Atlantique, Nantes Université, CNRS-IN2P3, Nantes, France
¹⁰⁵ Sungkyunkwan University, Suwon City, Republic of Korea
¹⁰⁶ Suranaree University of Technology, Nakhon Ratchasima, Thailand
¹⁰⁷ Technical University of Košice, Košice, Slovak Republic
¹⁰⁸ The Henryk Niewodniczanski Institute of Nuclear Physics, Polish Academy of Sciences, Cracow, Poland
¹⁰⁹ The University of Texas at Austin, Austin, Texas, United States
¹¹⁰ Universidad Autónoma de Sinaloa, Culiacán, Mexico
¹¹¹ Universidade de São Paulo (USP), São Paulo, Brazil
¹¹² Universidade Estadual de Campinas (UNICAMP), Campinas, Brazil
¹¹³ Universidade Federal do ABC, Santo Andre, Brazil
¹¹⁴ University of Cape Town, Cape Town, South Africa
¹¹⁵ University of Houston, Houston, Texas, United States
¹¹⁶ University of Jyväskylä, Jyväskylä, Finland
¹¹⁷ University of Kansas, Lawrence, Kansas, United States
¹¹⁸ University of Liverpool, Liverpool, United Kingdom
¹¹⁹ University of Science and Technology of China, Hefei, China
¹²⁰ University of South-Eastern Norway, Kongsberg, Norway
¹²¹ University of Tennessee, Knoxville, Tennessee, United States
¹²² University of the Witwatersrand, Johannesburg, South Africa
¹²³ University of Tokyo, Tokyo, Japan
¹²⁴ University of Tsukuba, Tsukuba, Japan
¹²⁵ University Politehnica of Bucharest, Bucharest, Romania
¹²⁶ Université Clermont Auvergne, CNRS/IN2P3, LPC, Clermont-Ferrand, France
¹²⁷ Université de Lyon, CNRS/IN2P3, Institut de Physique des 2 Infinis de Lyon, Lyon, France
¹²⁸ Université de Strasbourg, CNRS, IPHC UMR 7178, F-67000 Strasbourg, France, Strasbourg, France
¹²⁹ Université Paris-Saclay Centre d'Etudes de Saclay (CEA), IRFU, Département de Physique Nucléaire (DPhN), Saclay, France
¹³⁰ Università degli Studi di Foggia, Foggia, Italy
¹³¹ Università del Piemonte Orientale, Vercelli, Italy
¹³² Università di Brescia, Brescia, Italy
¹³³ Variable Energy Cyclotron Centre, Homi Bhabha National Institute, Kolkata, India
¹³⁴ Warsaw University of Technology, Warsaw, Poland
¹³⁵ Wayne State University, Detroit, Michigan, United States
¹³⁶ Westfälische Wilhelms-Universität Münster, Institut für Kernphysik, Münster, Germany
¹³⁷ Wigner Research Centre for Physics, Budapest, Hungary
¹³⁸ Yale University, New Haven, Connecticut, United States
¹³⁹ Yonsei University, Seoul, Republic of Korea
¹⁴⁰ Zentrum für Technologie und Transfer (ZTT), Worms, Germany
¹⁴¹ Affiliated with an institute covered by a cooperation agreement with CERN
¹⁴² Affiliated with an international laboratory covered by a cooperation agreement with CERN.